TÉCNICO LISBOA

Modeling of heat transfer in a combustion chamber and multiphase flow in a pilot-scale CFB

Agata Katarzyna Widuch

Thesis to obtain the Master of Science Degree in

Energy Engineering and Management

Supervisors: Prof. Pedro Jorge Martins Coelho

PhD Dsc Wojciech Adamczyk

Examination Committee

Chairperson: Prof. Edgar Caetano Fernandes

Supervisor: Prof. Pedro Jorge Martins Coelho

Member of the Committee: Prof. Viriato Sérgio de Almeida Semião

September 2019

Contents

Abstract

Fluidization process progressively gains interest. It is mainly due to high heat transfer and mixing rate of solid material. It is used for drying, cooling, mixing, and converting fuel energy into heat. The last of mentioned application is intensively developed in the energy sector. In case of building new units or improving the existing one, an extensive engineering work is required. In order to overcome necessity of performing on-site or laboratory test a numerical techniques can be used. Computational methods give great opportunity to predict and understand complex physical mechanisms. Industrial boilers, where fluidization technology is used, have high efficiency, leads to reduce emissions of harmful substances such as SOx and NOx along with the use of larger range of burnt fuel, including wastes. Nevertheless application of numerical techniques for predicting complex particle transport in dense solid flow is not a trivial task and requires special treatment and attention. This situation is mostly caused by intensive mixing, mutual particle interaction and strong coupling between phases. Modeling of multiphase flows can be done using Euler-Euler, hybrid Euler-Lagrange approaches as well as Discrete Element Method (DEM). The DEM technique takes into account collisions between particles applying direct collision model while remaining approaches model the collision using the idea of kinetic theory of granular flow. In contrary to Euler-Euler technique, DEM is not well tested yet for fluidization processes, mainly due to the cost of simulations. In this work, the potential of using the DEM for modeling combustion and heat transfer in fluidized bed was tested. Also, a comparison between data resulting from experiments on pilot-scale Circulating Fluidized Bed unit, Euler-Lagrange approach and DEM will be provided.

Key words: Computational Fluid Dynamics, Discrete Element Method, Fluidized Bed, Combustion, Heat Transfer

Resumo

Os processos de fluidização têm suscitado cada vez mais interesse. Isto é devido principalmente à elevada taxa de transferência de calor e de mistura do material sólido. Estes processos são usados para secagem, arrefecimento, mistura e conversão de energia química em energia térmica. Esta última aplicação é muito utilizada no setor energético. No caso da construção de novas unidades ou do melhoramento de unidades em operação, é necessário um extenso trabalho de engenharia. Para obviar à necessidade de realizar ensaios experimentais na própria unidade ou em laboratório, podem ser usadas técnicas numéricas. Os métodos computacionais oferecem grande potencial para prever e compreender mecanismos físicos complexos. As caldeiras industriais, onde a tecnologia de fluidização é utilizada, têm elevada eficiência, reduzindo as emissões de substâncias nocivas, como o SOx e o NOx, e permitem queimar uma maior variedade de combustíveis, incluindo resíduos. No entanto, a aplicação de técnicas numéricas para prever o fenómeno complexo do transporte de partículas sólidas num meio denso não é uma tarefa trivial e requer tratamento e atenção especiais. Esta situação é causada principalmente pela mistura intensa, pela interação entre as partículas e pelo forte acoplamento entre as fases. A modelação de escoamentos multifásicos pode ser feita usando métodos de Euler-Euler, métodos híbridos de Euler-Lagrange, bem como o Método dos Elementos Discretos (DEM). As técnicas DEM levam em consideração as colisões entre partículas aplicando o modelo de colisão direta, enquanto as restantes abordagens modelam a colisão usando a ideia da teoria cinética do escoamento granular. Ao contrário da técnica de Euler-Euler, o DEM ainda não foi bem testado para processos de fluidização, principalmente devido ao custo das simulações. Neste trabalho, testou-se o potencial do uso do DEM para modelar a combustão e a transferência de calor em leito fluidizado. Além disso, é feita uma comparação entre os dados experimentais em unidades de leito fluidizado circulante à escala piloto e resultados computacionais usando as abordagens Euler-Lagrange e DEM.

Palavras-chave: Mecânica dos Fluidos Computacional, Método dos Elementos Discretos, Leito Fluidizado, Combustão, Transmissão de Calor

List of Tables

List of Figures

Nomenclature

LATIN

A	area, m^2
C	molar concentration, $kmol/m^3$
C_D	drag coefficient
c	specific heat, J/kgK
D	abscissas, m
D_0	diffusion rate coefficient, m^2/s
D_m	diffusivity, m^2/s
d	particle diameter, m
e	restitution coefficient
F	force, N
f_{loss}	loss factor
$\mathbf{g}$	gravity vector, m/s^2
$g_{0,ss}$	radial distribution function
H	height, m
h	heat transfer coefficient, W/m^2K
h_{fg}	latent heat, J/kg
I_{2D}	second invariant of the deviatoric stress tensor
K	interphase exchange coefficient, kg/m^3s
k	thermal conductivity, W/mK
k_c	mass transfer coefficient, m/s
M	molecular weight, kg/kmol
m_p	single particle mass, kg
$\dot{m}$	mass flow rate, kg/s
N_{H_2O}	molar flux of vapor, $kmol/m^2s$
N_p	number of particles in parcel,
p	pressure, Pa
R	universal gas constant, J/kmolK
$\mathcal{R}$	kinetic rate coefficient, m^2/s
r	radius, m
S_b	stoichiometric burnout ratio, kg_{O_2}/kg_C
S_{mass}	source term due to exchange of mass, kg/m^3
S_{mom}	source term due to exchange of momentum, N/m^3
$S_{f,rad}$	source term due to radiation, W/m^3
$S_{f,rec}$	source term due to amount of energy released from chemical reactions, W/m^3
S_{en}	source term due to energy, W/m^3
S_p	source term due to species, kg/m^3
T	temperature, K
t	time, s
Qc	evaporation rate, m^2/s
$\mathbf{u}$	velocity vector, m/s
$\mathbf{v}$	velocity vector, m/s
X	mole fraction, $kmol_i/kmol$
x	positions of centers of particles, m
Y	mass fraction, kg_i/kg

GREEK SYMBOLS

α	thermal diffusivity, m2/s
η	coefficient of restitution for the dashpot term
γ	damping coefficient
Δt	time step size, s
δ	overlap, m
ε	phase fraction,
λ	air excess ratio
λ_s	bulk viscosity, kg/ms
Θ	granular temperature, m^2/s
μ	dynamic viscosity, kg/ms
ν	kinematic viscosity, m^2/s
Φ	angle of internal friction, rad
ρ	density, kg/m^3
τ_t	thermal response

DIMENSIONLESS GROUPS

Nu	Nusselt number, hd/k
Pr	Prandtl number, ν/α
Re	Reynolds number, ud/ν
Sc	Schmidt number, ν/D_m,
Sh	Sherwood number, hd/D_m

INDICES

cell	cell properties
coll	collision
en	energy
ext	external
f	gaseous/fluid phase
mass	mass
mf	minimum fluidization
s	solid phase
tf	terminal fluidization

ABBREVIATIONS

2D	Two-dimensional
BFB	Bubbling Fluidized Bed
CFB	Circulating Fluidized Bed
CFD	Computational Fluid Dynamics
DDPM	Dense Discrete Phase Model
DEM	Discrete Element Method
DPM	Discrete Phase Model
HEL	Hybrid Euler-Lagrange
KTGF	Kinetic Theory of Granular Flow
LHV	Lower Heating Value
LUT	Lappeenranta University of Technology
MPIC	Multiphase Particle-in-Cell
PSD	Particle Size Distribution
RDF	Refuse Derived Fuel
UDF	User Defined Function
POD	Properly Orthogonally Decomposed
RBF	Radial Basis Functions

1. Introduction

1.1. Fluidization

Fluidization is a multiphase process, where solid material is transported by flowing gas. The process in the last few decades has gained more and more interest. The technology finds application in many different industries, i.e. chemical for re-drying of chemicals after mechanical drying, pharmaceutical (e.g. medication mixing fluidization gives higher efficiency and more uniform distribution of material in comparison to mechanical mixing), food processing (popcorn popper) and many applications in the energy sector.

The last mentioned application is intensively developed. Intensive heat transfer, mixing of the solid material, long residence time of the fuel, or the uniform temperature distribution over the combustion chamber are the main factors that characterize this technology. The industrial boilers that use fluidization techniques have higher efficiency, even 10% higher in comparison with pulverized coal boilers. This is caused mainly by the high mixing rate which affect all thermochemical processes that occur during coal combustion, for instance this helps in reduction of SOx emission by direct limestone injection.

The combustion temperature in fluidized bed ranges between $800-950°C$, which accounts for lower NOx emissions, allows to burn fuel (as wastes) with lower heating value [1]. Lower temperature results in no softening of an ash, that further does not create problems with slag or coating formation on a chamber walls that will lead to decrease of heat transfer rate between the heating surfaces and the heated medium [2].

Another advantage of the usage of this type of boilers is their low sensitivity to fuel quality. A large range of fuel types, including wastes can be easily burned. Looking to the proportions of the material transported in the combustion chamber, the coal fraction is only 3% of the total material in the combustion chamber, the rest is the inert material. The purpose of the inert material is to transfer the heat released during combustion process [3].

As it was mentioned the fluidization is a process where due to gas flow through the chamber, the suspension of solid particles in the fluid switches them into a fluid-like state. The process begins putting material on the porous plate. Then gas with low flow rate starts passing through the porous plate and material. The minimal fluidization velocity of a gas (u_{mf}) is reached once the gravitational and other forces affecting particles are balanced and they start to move (Fig. 1a). Continuing the increase of velocity above the minimal fluidization velocity rises smaller particles to the top of the boiler and gas bubbles appear (Fig. 1b). Exceeding of so called terminal velocity (u_{tf}) bubbles vanish, instead turbulent motion of particles occur (Fig. 1c). Further increase of gas velocity transforms the turbulent bed into a circulating fluidized bed. Particles are removed through the top part of the chamber and after passing over the solid separator return to the chamber (Fig. 1d).

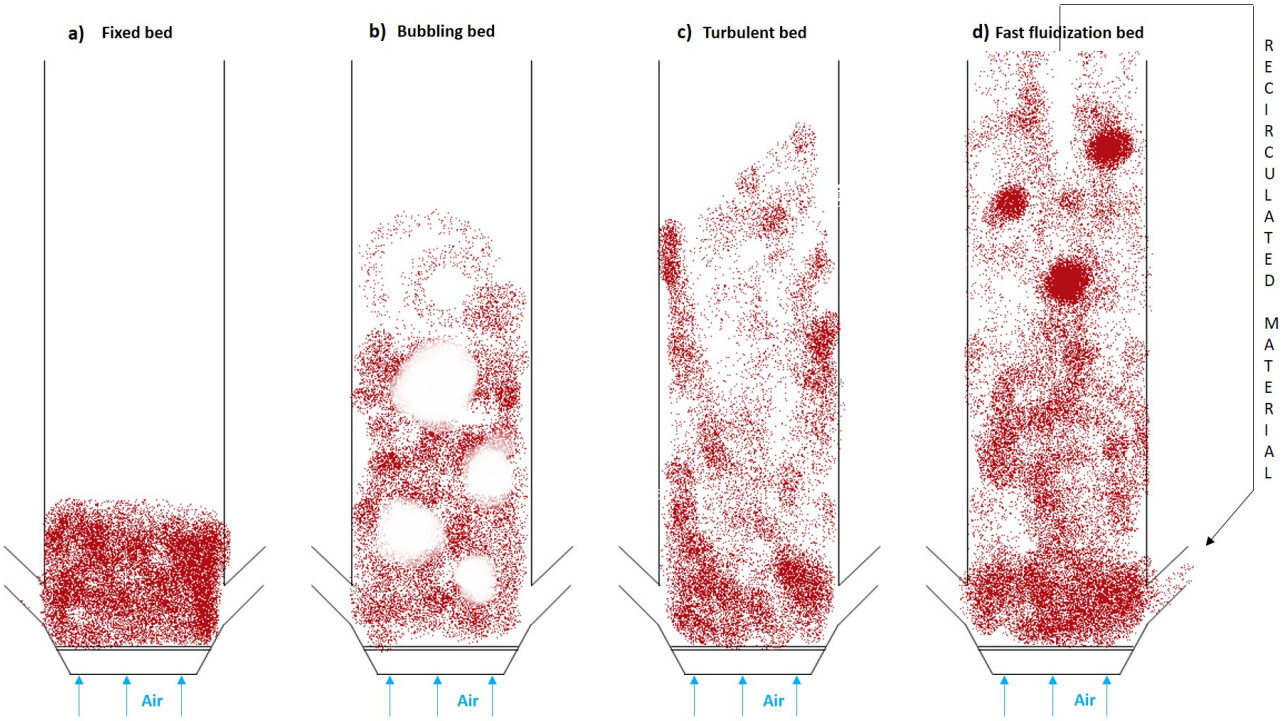

Figure 1: Fluidization regimes

1.2. Fluidization regimes

In a fluidized bed boiler, three characteristic zones can be recognized: dense, transition and dilute (see Fig. 2). The greater the distance from the gas distributor the lower the concentration of particles. In the dense zone creation of the fluidized bed starts. Due to high volume concentration particles are accumulating into so called clusters, where the interaction between solid material is an effect of friction forces. Because of the small distance between particles in this zone, collisions do not play an important role. The clusters expand to the transition zone as a result of friction and kinetic transport. When the distance between particles in the higher part of a boiler increase, the collisions take over dominance. Kinetic transport starts to dominate when the distance between particles gets large. Particle size and density as well as overall mass of material in a boiler influences not only the minimum fluidization velocity but also the size of particular zones. Particles with smaller diameter are easily moving to the upper parts of a boiler.

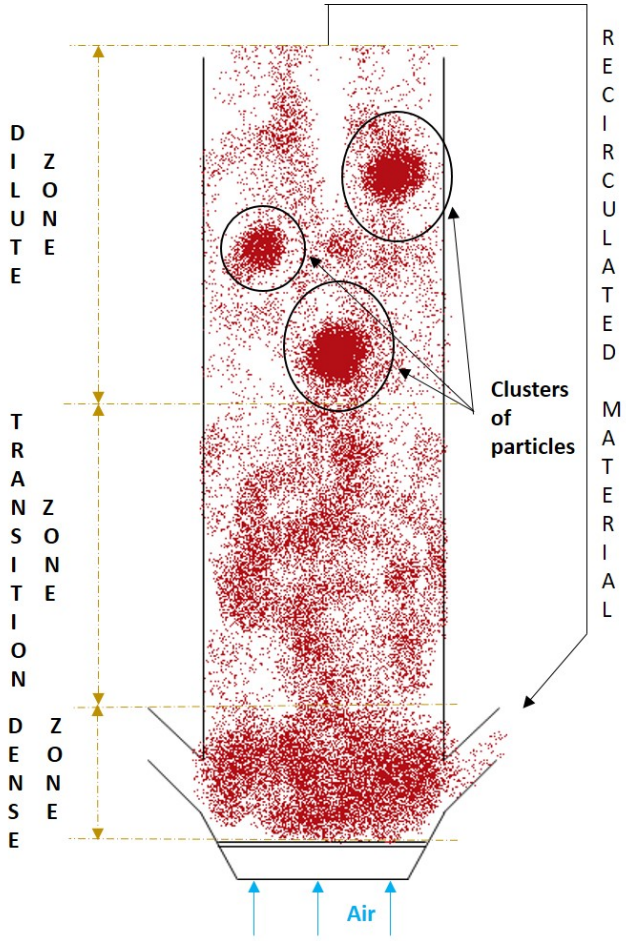

Figure 2: Fluidization zones

1.3. Bubbling Fluidized Bed

In comparison to Pulverized Coal Fired (PC) boilers, Bubbling Fluidized Bed (BFB) operates at lower temperatures 800℃-950℃. The combustion chamber is the main part of the BFB boiler, where conversion of fuel into heat is held. Depending on the desired output hot water or steam can be produced. The material of bed is the mixture of fuel and inert material, which is a common feature for all fluidized beds. An addition of limestone used for sulphur capture is also routinely used.

Before starting combustion the bed material has to be mixed with fuel. The bed material is composed of fuel and inert material-usually sand with addition of limestone. In the BFB boiler two locations of supplied air are present - at the bottom of the chamber and above the combustion zone (see Fig. 3). Providing air from underneath ensures proper mixing of inert material with coal. The gas velocity constantly changes and is kept in a range between the minimum fluidization velocity and the entrainment velocity [4]. Residues of burnt fuel in the form of ash with a small diameters are removed from the combustion chamber through the orifices. The greatest values of heat fluxes in the BFB boilers are at the bottom. In order to protect them from erosion and water dry-out the internal surface is covered by appropriate refractory material [5].

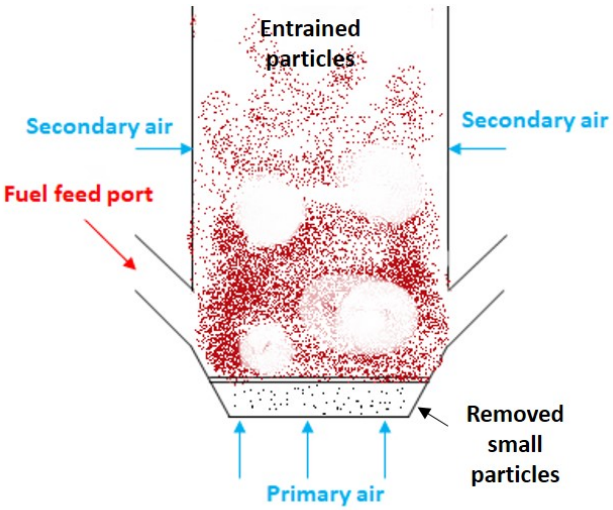

Figure 3: Closure to the bottom of BFB boiler

1.4. Circulating Fluidized Bed

Among the fluidization technology, nowadays the most popular is the Circulating Fluidized Bed (CFB). The main advantage of such boilers is their insensitivity to fuel quality. Due to relatively low combustion temperature fuel with higher moisture content, lower heating value fuels can be burnt in the CFB boiler. Those properties characterize biomass or RDF (Refuse Derived Fuel). This is of a great importance where challenge with waste management is constantly increasing. The CFB boilers are mainly dedicated for units of high generating power. Already installed, example units, have electrical power of 460 MWe (Łagisza, Poland), 330 MWe (Novocherkasskaya, Russia) and 550 MWe (Samcheok, South Korea) [6].

The particle resistance time, due to the close loop is much longer in comparison to the traditional pulverized coal boilers. Instead of removal of not burnt fuel particles, they are separated from flue gases and returned to the combustion chamber through separator and loop seal. High conversion rate of fuel results in higher boiler efficiency. It has to be taken into account that co-combustion of different types of fuels is possible and also function properly. The amount of oxidizer provided to the combustion chamber, within different zones need to be adjusted for the type of fuel, taking into account its size, density and moisture content. One of the operating conditions is the velocity, which needs to be maintained over the entrainment velocity ranging from 4.5 to 6.7 m/s [7]. This allows to uplift particles and redistribute them uniformly in the chamber - lighter particles are raised and heavier are occupying the bottom part of the chamber until fragment into the smaller ones during collision, particle swell, and breakage processes. A typical CFB boiler scheme is shown in figure 4 consists of the combustion chamber, loop-seal and drain section.

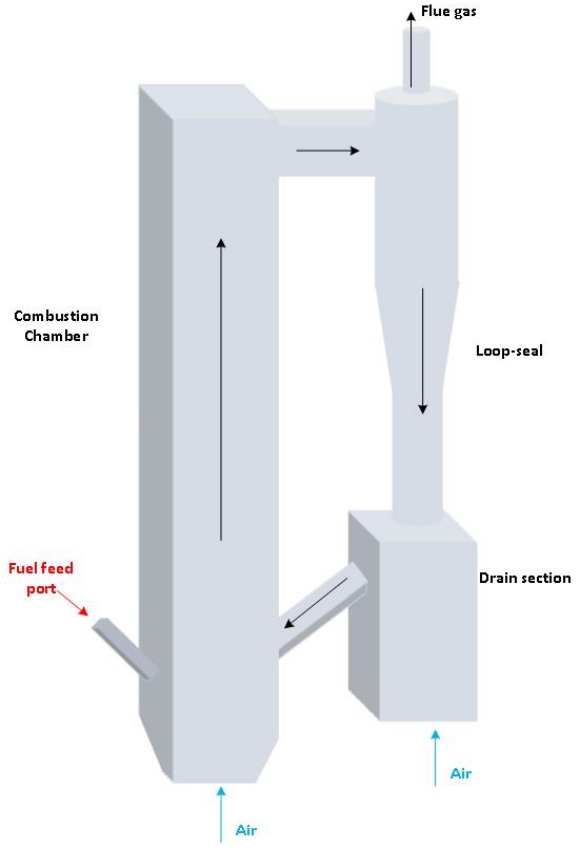

Figure 4: General scheme of the CFB boiler with higlighted injection ports

Primary air is supplied to the boiler through the oxidizer distributor (separator). The material in the chamber consists of fuel, inert material, sorbents. Injecting air with a speed exceeding the terminal velocity results in a highly turbulent bed. Another factor affecting the rate of turbulence is the shape of the boiler. The common technique is to construct boilers where the lower part is narrower than the upper. Particles are constantly carried out from the bottom of the boiler to the top to be as final returned back through loop seal and drain section to boiler. The height of rising of particles depends on their mass. If gravitational force is the prevailing force acting on the particle then it glides on walls and falls down. Due to high heat transfer and mixing rate, the temperature of combustion is uniform and lower (800℃−950℃) as well as heat fluxes to the boiler walls in comparison to PC boilers. Similar to the BFB boilers, the internal surface of the CFB boiler walls is covered by refractory material in order to protect them from high heat fluxes occurring inside the combustion chamber.

1.5. The particle hydrodynamics

The hydrodynamic interactions between the gas and solid (dispersed) phases are responsible for the complexity of the gas-solid flows. The hydrodynamic forces can be decomposed into several groups. The gravitational force is balanced by the fluid drag and buoyancy forces which act in opposite direction. When those forces are in pseudo-equilibrium state, the particle is suspended in carried gas. The medium within the fluidized bed behaves then as if it were a fluid, and can be described by mathematical tools developed to deal with the continuous phase:

- the static pressure at any height in the vessel is approximately equal to the weight of the solid bed per unit of cross-sectional area above that level where the pressure acts,
- an object which has higher density than the density of the bed will sink, while the lighter objects will float following Archimedes principle,
- the solids from the bed may be drained like a liquid through an orifice at the bottom or on the side of the container,
- the bed surface maintains a horizontal level, independent how the container is tilted, moreover the bed assumes the shape of vessel,
- for well mixed particles the bed maintains a nearly uniform temperature when heated.

An example where the differences between solid and fluid flow can be noticed is an *hour-glass* and a *U-tube pipe*. Within the hour-glass, the particle flow rate through the orifice in the bottom is constant and independent of particle bed height. This is an opposite to the fluid where the flow rate through the oriface depends on the hydrostatic pressure, while in the U-tube when it is filled by the fluid both arms contain the same amount of water, whereas when instead of fluid the sand will be used, only one arm of the U-tube is filled.

The pressure drop across the bed results from the drag forces acting on the particles immersed in moving fluid. The pressure drop per unit height of a packed bed $\Delta p/H$ with uniformly sized particles can be correlated using Ergun equation [8]

$$\frac{\Delta p}{H} = \underbrace{\left[150\frac{(1-\varepsilon_f)^2}{\varepsilon_f^3}\frac{\mu_f}{(k_v d_p)^2} + 1.75\frac{\rho_f(1-\varepsilon_f)u_f}{\varepsilon_f^3 d_p k_v}\right]}_{K_{fs}} u_f \tag{1}$$

where term K_{fs} is the interphase exchange coefficient between phases, ε_f stands for the void fraction of the bed, d_p represents the diameter of the particles, u_f is the superficial velocity of the gaseous phase, i.e., velocity that the fluid would have through the empty tube at the same volumetric flow rate, H defines the bed height and k_v is the particle sphericity which for ideal sphere is equal to $\pi/6$.

With increasing the pressure drop in the solid bed, the superficial gas velocity u_f tends to a critical value known as the minimum fluidization velocity u_{mf}. For a bed at rest the pressure drop can be defined as [9]

$$\Delta p = H(1-\varepsilon_f)(\rho_p - \rho_f)g \tag{2}$$

where H stands for the height of the bed, ρ_p is the particle density and g - the acceleration of gravity. The minimum fluid velocity u_{mf} at which the bed starts to fluidize, can be calculated by solving simultaneously equations (1) and (2) assuming $u_f = u_{\mathrm{mf}}$.

Other important velocities which are responsible for particle transport phenomena in fluidized bed are the terminal velocity u_{tf} and relative velocity u_{r}. The terminal velocity can be calculated from particle force balance

equation (3) under assumption, that the gas velocity u_f is equal to zero, and particle velocity u_p is equal to terminal velocity u_{tf}. Particle balance equation (3) has been derived for a single particle movement under gravitational, buoyancy and drag forces.

$$\underbrace{m_p g}_{\text{Gravity}} = \underbrace{m_p \frac{\rho_f g}{\rho_p}}_{\text{Buoyancy}} + \underbrace{C_{\mathrm{D}} \frac{\pi \left(u_f - u_p\right)^2 \rho_f}{8} d_p^2}_{\text{Drag}} \tag{3}$$

In equation (3) $(u_f - u_p)$ defines the relative velocity (slip velocity, u_{r}), which represents particle resistance against falling, when the gas and particle move upwards, C_{D} is the drag coefficient.

In multiphase flows where solid phase is relatively diluted $(1 - \varepsilon_f) < 0.1$ one- and two-way coupling between phases come into play [4]. For such cases the interactions between particles can be omitted. In one-way coupling the gaseous phase affects the particle motion, while there is no reverse effect of the particle movement on the fluid. Should both direction of influence be accounted for, the coupling is termed two way coupling.

2. Scope of the Thesis

In any circumstances where new units will be built or the existing one requires improvements, an extensive engineering work is required. Environmental regulations are constantly forcing energy sector to develop new techniques of converting fossil fuels into high energy forms. CO_2 content in the atmosphere is constantly increasing mainly due to combustion of fossil fuels, which leads to increase of overall temperature. Due to this new alternatives have to be found. Fludized bed might be a support for renewable sources of energy as fan mills, solar panels, water wind farms since operating of those forms is strictly dependant on weather conditions. Even though they are green solutions their efficiency is not high, it varies from 18 % to 30.5 % [10, 11].

In order to overcome necessity of performing on-site or laboratory tests a numerical techniques can be used. The application of Computational Fluid Dynamics (CFD) seems to be the most suitable one. The fluidization is an example of physical process that can give engineers sleepless nights. Mostly, due to the complexity of the mathematical models that is used for description of phase interaction processes. To achieve high accuracy of the model as well as appropriate definition for model coefficient experimental data is required. Before model application for large scale boilers, low level experiments which give possibility to validate submodels need to be carried out. Besides a wide application of the fluidization process, due to its complexity, is seen as one of the most challenging process for mathematical modeling. The chemical processes, the presence of various spatial and temporal scales, strong coupling between the gaseous and solid phases, and mutual interactions between particles make development of a reliable mathematical model for simulating fluidization process not a trivial task. The presence of combustion, gasification, particle fragmentation, attrition and agglomeration makes the task even more demanding. One of the grand challenges is the need of accurate, fast, robust and stable computing tool for predicting/modeling particle fluidization process. The available computational techniques capable of dealing with such a complex process can be divided into four main groups:

- microscale: discrete element model, discrete numerical simulation, etc.
- macroscale empirical and semi-empirical models,
- meso- and macroscale multifluid models like Euler–Euler models,
- macroscale hybrid Euler–Lagrange (HEL) models (known also as the multiphase particle-in-cell (MP-PIC) method)

Because each of these techniques have certain drawbacks there is still plenty of room for their improvement by enhancing the numerical modeling capabilities. The engineering community needs to face a grand-challenge in future years, namely the development of a validated, predictive, robust, multi-scale modeling tool, to enhance the modeling capabilities by reduction of computational effort. The computational methods give great opportunity to predict and understand complex physical mechanisms standing behind the fluidization process.

The accurate prediction of collisions between particles allows to determine the best distribution of material in a bed precise determination of pressure profiles, drag forces and zones of intensive errosion. One of the grand challenges in modeling fluidization process is the need of accurate, robust, fast and stable numerical model for predicting the collision between particles in dense systems. Such systems are encountered e.g., in fluidized bed boiler (used in waste management, energy and environmental sectors), pressurized solid gasifiers, etc. Without such model it is difficult to achieve reliable predictions of the solid distribution within the system. This in turn, has a direct impact on predicted pressure profile, temperature distribution, harmful species reduction, predicted solid separation efficiency, prediction of erosion, etc., where these problems have been addressed in [12, 13, 14]. Available techniques like Granular Euler-Euler (EE), hybrid Euler-Lagrange (HEL), Discrete Element Model (DEM: Soft or Hard Sphere) suffer from some difficulties. The most problematic are:

- long calculation time for DEM approach,
- problem with predicting Granular Temperature (GT) (Θ – used in all closure terms of the collisional and phase interaction models) in both EE and HEL techniques,
- problem with predicting particle size distribution in case of using EE approach (each particle size represented by additional solid phase),
- high instability of the solution procedure when the number of particle in the system reaches a large number (over 3 M) in HEL approach,
- problem with conservation of mass in its interpolation from discrete phase to Eulerian grid when HEL technique is used (problem partially resolved in MP-PIC approach – commercial CPFD Software, LLC Barracuda code), etc.

To address the solution of such problems the engineering community involved in the modeling of particle transport will need to go through profound innovations in the future years, to develop modeling strategies for the prediction of the fluidization, which will be able to accurately resolve particle-particle interaction in a reasonable time frame. To develop accurate model a multiscale modeling approach of the fluidization process needs to be used. The particle collisions need to be predicted at the micro-scale level while the particle transport should be modelled at meso- and macro-scales [15] which is illustrated in Fig. 5. To this end, there is an urgent need for reliable and adaptive Reduced Order Model (ROM) for prediction of the particle-particle collision, that will allows the use of numerical tool in realistic time-frame in the case of application for large fluidized systems.

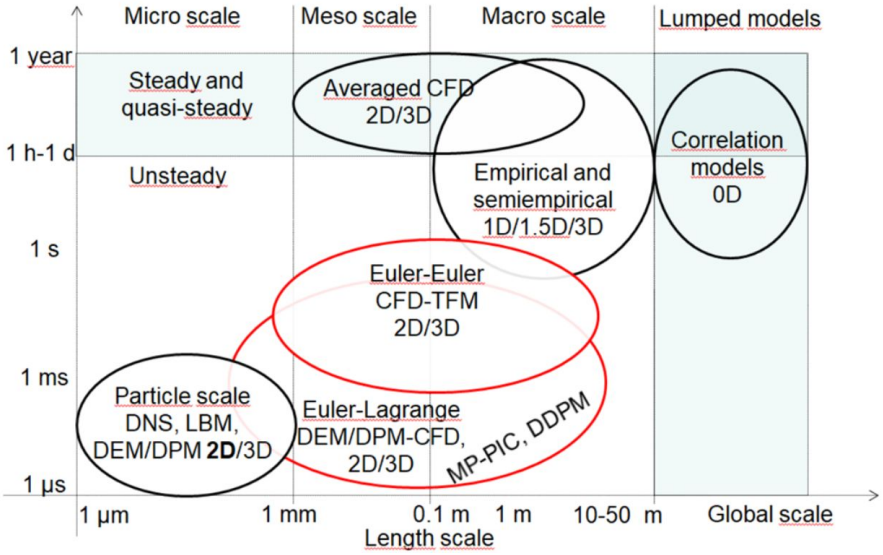

Figure 5: Classification of multiphase models for fluidized systems (reproduced from: [15])

Usually two main approaches are used for simulations of fluidization. The first one is the Euler-Euler approach [16, 9, 17]. In this approach, both dispersed and continuous phases are treated as interpenetrating continua. This approach has been developed assuming that the solid phase can be treated as acontinuous medium with representative properties similar to the fluid [16]. The first derivation of the equations for two-phase systems can be found in Anderson and Jackson [18]. The application of two-fluid model for modeling particle transport phenomena needs definition of closure models. The functionality of these models are the predicting of the particle collisions, the fluid-solid interaction. Applying the theory of dense gases [19] particles interactions can be predicted based on kinetic theory of granular flow (KTGF) [20]. An additional disadvantage of the Eulerian model is the necessity of using a fine mesh for accurate modeling cluster formation what results in long computational time and affect the calculated pressure profile along the combustion chamber.

A straightforward approach for modeling particle interactions is application of the discrete particle techniques. The discrete models applied to dense dispersed phase in the fluidized bed boiler can accurately predict particles and particle fluid interaction and the Particle Size Distruibution (PSD) in dispersed phase. This can be achieved by using the Discrete Element Method (DEM) [4]. This two approaches describe the particle interaction using the hard-sphere and soft-sphere collision models. The hard-sphere model assumes that interactions between particles are instantaneous [21]. The particle collision effect is identified between each of the particle pairs, which is numerical expensive. The soft-sphere model uses the Hertzian contact theory, which models slight overlapping of particles during contact [22]. Due to the intensive calculations, the usability of the DEM is limited to small scale problems. Some applications of the hard-sphere DEM for modeling of particle transport in small-scale fluidized beds can be found in [23], whereas Tsuji et al. [24] used the soft-sphere collision model for simulating bubbling fluidized bed, employing 4.5 millions of particles. Even with the increasing computer power DEM is numerically very expensive.

The next approach that can be used for modeling the fludization process taking into account real PSD is the hybrid Euler-Lagrange technique, where in contrary to Eulerian technique the fluid-phase is treated as continuum, while the solid phase is tracked in a Lagrangian reference frame. In order to speed up the numerical simulation without losing accuracy, a hybrid Euler-Lagrange approach has been developed by Andrews and

O'Rourke [25]. This method was later enhanced by Patankar [26, 27] and Snider [28, 29, 30]. For simplification of calculations particles are packed in parcels with specified mass, diameter and density but corresponding to particles behaviour. The particle – particle interactions are not simulated directly, but are accounted for by means of the KTGF in the Eulerian frame, where the particles are projected [31].

2.1. Objectives

There are two main objectives of the thesis. The first one is to validate whether the DEM model can be successfully used for modeling heat transfer and mixing processes. In case of modeling fluidization process in CFB boilers an extremely important issue is the modeling of the solid combustion process. This is not a trivial task, even in modeling combustion of gaseous fuel, while the presence of dense two phase flow with strong interactions between phases, modeling of the combustion of solid fuel is not simpler. To check how the DEM approach deals with combustion several simulations have been carried out, using two configurations of the coal injection ports. The set of results was also compared with an analytical solution, using flue gas composition and energy balance. The great question in case of modeling fluidization process arises in terms of the numerical model stability and robustness. To ensure this is even more complicated in the presence of a reacting flow.

The last but not least part of the thesis is focused on the application of the DEM approach for modeling the particle transport in the pilot-scale test rig built at Lappeenranta University of Technology [32]. This pilot installation is ideal for providing data for testing the accuracy of the numerical models. In the earlier work measured pressure profiles along the riser were used for validation the hybrid Euler-Lagranage technique. In the presented work this data has been used for testing the DEM approach, mainly the effect of particle size on the predicted pressure profile.

It is worth to mention here that the work carried out consists an enormous source of knowledge for understanding the implementation of the DEM model to Ansys Fluent [33]. Moreover, carried out test will be used for testing the collisions model that will be developed in an ongoing project at the Silesian University of Technology founded by National Science Center.

2.2. Structure of the Thesis

The thesis contains 5 chapters. In the first chapter general information about the fluidization phenomena, its advantages and revision of models possible to use to simulate it together with objectives of work. In the second chapter, a brief description of the methods avaliable to simulate fluidization process is given together with different types of fluidized beds. The third chapter covers issues related to used mathematical model with governing equations. A forth chapter is divided into two sub chapters; the first one concerns heat transfer and combustion with mixing processes, while the second one concerns modeling multiphase flow in a pilot-scale rig. Last but not least chapter consists conclusions regarding the obtained results and possible further use of the DEM model in large scale installations.

3. Mathematical model

The numerical modeling of the fluidization processes in large scale installations as well as in the laboratory devices is computationally complex and very expensive. As it was mentioned earlier, different models are available to simplify and speed up numerical simulations. Nevertheless, all of them suffer from some deficiencies, mainly concerning the accuracy of prediction of the particle-particle collisions. In order to accurately resolve this problem, the Discreet Element Model (DEM) soft sphere model may be used. Therefore, approach which gives possibility to reduce calculation time without losing accuracy is very desirable. In order to deal with the aforementioned difficulties new approach for predicting particles collision has to be developed in future.

The present thesis investigates the possible application of a complex collision model based on the DEM approach for modeling laboratory scale CFB installation. Moreover, the heat and mass transfer aspects in case of use the DEM technique will be investigated. The core of the DEM approach for modeling fluidization process where strong interaction between gaseous and solid phase need to be taken into account is the coupling between phases. In this model the same strategy as in application of Dense Discreet Phase Model (DDPM), named also hybrid Euler-Lagrange (HEL) technique is used. The next section describes basic features and equations resolved by the DDPM approach. Next, the collision model used by the DEM technique is described which is an extension of the DDPM approach while the KTGF collision approach is replaced by the direct collision one.

3.1. Hybrid Euler-Lagrange model

For the hybrid Euler - Lagrange approach, the mass, momentum, energy and species transport equations together with the turbulence model need to be solved. The mass, momentum, energy and species transport equations for the gaseous phase in instantaneous form are written as [33] [34]:

$$\frac{\partial}{\partial t}\left(\varepsilon_f \rho_f\right) + \nabla \cdot \left(\varepsilon_f \rho_f \mathbf{u}_f\right) = S_{\text{mass}} \tag{4}$$

$$\frac{\partial}{\partial t}\left(\varepsilon_f \rho_f \mathbf{u}_f\right) + \nabla \cdot \left(\varepsilon_f \rho_f \mathbf{u}_f \mathbf{u}_f\right) = -\varepsilon_f \nabla p + \nabla \cdot \tau_f + + \varepsilon_f \rho_f \mathbf{g} + K_{DPM}\left(\mathbf{u}_s - \mathbf{u}_f\right) + S_{\text{mom}} \tag{5}$$

$$\frac{\partial}{\partial t}\left(\varepsilon_f \rho_f h_f\right) + \nabla \cdot \left(\varepsilon_f \rho_f \mathbf{u}_f h_f\right) = \varepsilon_f \frac{\mathrm{D}p}{\mathrm{D}t} + \tau_f : \nabla \mathbf{u}_f - \nabla \cdot \mathbf{q}_f - \nabla \cdot \left[\sum_{k=1}^{m} \varepsilon_f h_{f,k} \mathbf{J}_k\right] + S_{f,\text{rad}} + S_{f,\text{rec}} + S_{\text{en}} \tag{6}$$

$$\frac{\partial}{\partial t}\left(\varepsilon_f \rho_f Y_{f,k}\right) + \nabla \cdot \left(\varepsilon_f \rho_f \mathbf{u}_f Y_{f,k}\right) = \nabla \cdot \varepsilon_f \mathbf{J}_k + \varepsilon_f R_{f,k} + \mathcal{R} + S_{\text{sp}} \tag{7}$$

where the subscripts f and s denote the fluid and solid phase respectively, k - species index, h - enthalpy, $Y_{f,k}$ - mass fraction of species k in fluid phase, K_{DPM} - drag coefficient calculated for the average value of the solid volume fraction in a numerical cell, $\text{Sc}_{f,k}$ - Schmidt number, m - number of species in resolved flow, $\mathbf{J}$ - diffusion flux of species k, and $\mathbf{q}$ - heat flux. The source term $S_{f,\text{rad}}$ - the contribution to the energy equation due to the radiation. The source term $S_{f,\text{rec}}$ - the amount of energy released from chemical reactions. The $R_{f,k}$ - the net rate of production of homogeneous species k, $\mathcal{R}$ - the heterogeneous reaction rate in case of modeling surface combustion. The S_{mass}, S_{mom}, S_{en} and S_{sp} are sources due to exchange of mass, momentum energy and species between the continuous phases and particles in discrete phase, respectively. The energy source S_{en} consists of the enthalpy transfer due to convection, chemical reactions and radiation from discrete phase. The momentum source term S_{mom} determines the change of momentum in the gaseous phase due to particles movement.

The DDPM approach does not solve motion equation for individual particles, which is also the case of MP-PIC technique. The solver tracks groups of particles called parcels. Each parcel contains several particles of the

same mass, velocity, position, composition, etc. The number of individual particles contained in the injected parcel can readily be calculated from

$$n_p = \frac{\dot{m}_{\text{parcel}} \Delta t}{m_p} \tag{8}$$

where Δt is the time step in transient calculation, $\dot{m}_{\text{parcel}}$ mass flow rate of single parcel and m_p is the mass of individual particle evaluated based on the particle diameter and density. The particle equation of motion which equates the particle inertia with the forces acting on a particle, reads then

$$\frac{\mathrm{d}\mathbf{u}_p}{\mathrm{d}t} = F_{\mathrm{D}}(\mathbf{u}_f - \mathbf{u}_p) + \frac{\mathbf{g}(\rho_p - \rho_f)}{\rho_p} - \frac{\nabla p}{\rho_p} - \frac{\nabla \cdot \sigma_s}{\rho_p} \tag{9}$$

where subscript p denotes the particle data (in one dispersed phase several materials with different physical properties can be tracked). σ_s is the granular stress tensor which represents particles interactions calculated based on the KTGF [9] [19] in the Eulerian grid. ρ_p is the particle material density, $F_{\mathrm{D}}(\mathbf{u}_f - \mathbf{u}_s)$ is the particle acceleration due to the drag. The drag coefficient F_{D} is calculated using the same drag model as this used for predicting the drag coefficient K_{DPM}. The term $-\nabla p/\rho_p$ defines the particle acceleration due to the pressure difference at the particle location.
Based on the calculated particle velocity a new position of the particle is defined as

$$\frac{\mathrm{d}\mathbf{x}_p}{\mathrm{d}t} = \mathbf{u}_p \tag{10}$$

After obtaining the particle position, the solid volume fraction in a given numerical cell can be calculated as

$$\varepsilon_s = \frac{\sum_{i=1}^{N_{\text{parcels}}} V_{p,i} n_{\mathrm{p},i}}{V_{\text{cell}}} \tag{11}$$

where V_p is the considered particle volume, V_{cell} is the numerical cell volume, k_{v} defines the particle sphericity and d_p represents the particle diameter. The calculated solid volume fraction is assigned to Eulerian grid where the void fraction can be determined as $\varepsilon_f = 1 - \varepsilon_s$. The particle velocity and position obtained by solving Eqs. (9) and (10), strongly depends upon the evaluated solid stresses σ_s (see Eq. (12)) in the Eulerian grid. In order to calculate the solid stress tensor several closure terms have to be calculated.

In order to calculate the solid stress tensor σ_s, which accounts for interactions between particles within solid phase, several closure terms have to be defined. Closure terms are used in a description of the granular pressure, solid bulk viscosity and shear viscosities. The solid stress tensor can be defined as [20]

$$\sigma_s = -p_s \bar{\mathbf{I}} + \varepsilon_s \mu_s \left(\nabla \mathbf{u}_s + \nabla \mathbf{u}_s^T \right) + \varepsilon_s \left(\lambda_s - \frac{2}{3} \mu_s \right) \nabla \cdot \mathbf{u}_s \bar{\mathbf{I}} \tag{12}$$

where λ_s is the bulk viscosity, $\bar{\mathbf{I}}$ is the unit tensor, p_s is the granular pressure, μ_s represents the solid dynamic viscosity, and $\mathbf{u}_s$ stands for the average velocity vector of the solid phase acquired at the particle location. Further granular phase modeling requires mathematical description of the dynamic viscosity, bulk viscosity and the solid pressure. The flow regime occurring in the system, understood as the solid-solid momentum exchange mechanism occurring at different solid volume fractions, determines the dispersed phase modeling. Particle collisions and kinetic transport are of a great importance for low solid volume fractions. When the volume fraction for the particulate matter is high, the particle collisions are no longer instantaneous and therefore friction between particles and kinetic transport controls the transport. Thus, dynamic viscosity of the solid phase can be expressed as a superposition of three terms

$$\mu_s = \mu_{s,\text{kin}} + \mu_{s,\text{col}} + \mu_{s,\text{fric}} \tag{13}$$

in which $\mu_{s,\text{col}}$, $\mu_{s,\text{kin}}$, and $\mu_{s,\text{fric}}$ represent the viscosity due to collisions, kinetic transport and friction, respectively. Several models derived from the KTGF for calculating the granular viscosity can be found in literature. In this work, the following correlations representing the viscosities due to kinetic transport [9] and collisions [20] are applied

$$\mu_{s,\text{kin}} = \frac{\varepsilon_s \rho_s d_s \sqrt{\Theta\pi}}{6(2-e_{ss})}\left[1+\frac{2}{5}(1+e_{ss})(3e_{ss}-1)\varepsilon_s g_{0,ss}\right] \tag{14}$$

$$\mu_{s,\text{col}} = \frac{4}{5}\varepsilon_s^2 \rho_s d_s g_{0,ss}(1+e_{ss})\left(\frac{\Theta}{\pi}\right)^{1/2} \tag{15}$$

where e_{ss} represents the inelastic nature of particle collisions, known as the restitution coefficient, and Θ is the granular temperature. The restitution coefficient e_{ss} represents the fraction of energy locally dissipated due to particle-particle or particle-wall collisions. When a plastic collision occurs (total collision energy is dissipated) the restitution coefficient is equal to zero, whereas for an elastic collision (total collision energy is conserved) its value is equal to unity. The probability of particle collisions $g_{0,ss}$ can be calculated as [35]

$$g_{0,ss} = \left[1-\left(\frac{\varepsilon_s}{\varepsilon_s^*}\right)^{1/3}\right]^{-1} \tag{16}$$

where ε_s^* stands for the maximum packing limit of particles. The radial distribution function tends to infinity when a distance between particles approaches the value of particle diameter and tends to unity when the distance is increasing. When the solid volume fraction exceeds the defined transition limit (friction limit) ε_s^{fr}, the model dedicated for a dense regime (friction regime) is activated. In this regime the collision part of the solid viscosity is replaced by the friction viscosity $\mu_{s,\text{fric}}$ defined as [36]

$$\mu_{s,\text{fric}} = \frac{p_s \sin\phi}{2\sqrt{I_{2D}}} \tag{17}$$

where I_{2D} stands for the second invariant of the deviatoric stress tensor, ϕ is the angle of internal friction and p_s is the granular pressure. The granular pressure, similarly to granular viscosity, is split into three terms which represent the kinetic transport, collisions and friction. The relation for the granular pressure in case of dilute flows can be written as [37]

$$p_s = \varepsilon_s \rho_s \Theta + 2\varepsilon_s^2 \rho_s (1+e_{ss}) g_{0,ss} \Theta \tag{18}$$

where the first term represents the kinetic transport and the latter stands for the transport due to collisions. In dense regions, where the solid volume fraction exceed the transition volume fraction (friction limit) ε_s^{fr}, the term representing the collision pressure is replaced by the solid friction pressure $p_{s,\text{fric}}$ derived based on the KTGF theory [19] defined as

$$p_{s,\text{fric}} = 10^{25}(\varepsilon_s - \varepsilon_s^{fr})^{10} \tag{19}$$

The bulk viscosity present in Eq. (12) defines the resistance of solid body to dilatation and it can be modeled as [37]

$$\lambda_s = \frac{4}{3}\varepsilon_s \rho_s d_s g_{0,ss}(1+e_{ss})\sqrt{\frac{\Theta}{\pi}} \tag{20}$$

One of the most important parameters, which corresponds to interactions between gas and particles, is the drag exchange coefficient K between phases. The relationship representing the drag coefficient is typically obtained experimentally, based on the pressure drop measurements in fluidized or settling beds. In the current work the model proposed by Gidaspow [9] has been used. This approach combines two closure approximations, namely the Ergun model [38], which holds for solid volume fractions exceeding 0.2 and Wen&Yu model [39]

which is used in regions where solid volume fraction is sharply smaller than 0.2. The Ergun and the Wen and Yu models are given by Eq. (21) and Eq. (22), respectively

$$K_{\text{Ergun}} = 150\frac{\varepsilon_s^2\mu_f}{\varepsilon_s d_s^2} + 1.75\frac{\rho_f\varepsilon_s\left|\mathbf{u}_s - \mathbf{u}_f\right|}{d_s} \tag{21}$$

$$K_{\text{Wen\&Yu}} = 0.75C_{\text{D}}\frac{\varepsilon_s\varepsilon_f\rho_f\left|\mathbf{u}_s - \mathbf{u}_f\right|}{d_s}\varepsilon_f^{-2.65} \tag{22}$$

where C_{D} is the drag coefficient defined as

$$C_D = \frac{24}{\varepsilon_f \text{Re}}\left[1 + 0.15(\varepsilon_f \text{Re})^{0.687}\right] \tag{23}$$

A closer inspection of Eqs. (21) and (22) shows that there is a discontinuity at $\varepsilon_s = 0.2$ [40]. To overcome this difficulty, a blending function is frequently employed, making the model smooth. Thus the drag coefficient model can be written as [9]

$$K = \phi(\varepsilon_s)K_{\text{Ergun}} + (1 - \phi(\varepsilon_s))\,K_{\text{Wen\&Yu}} \tag{24}$$

where $\phi(\varepsilon_s)$ is the blending function defined as

$$\phi(\varepsilon_s) = 0.5 + \frac{\arctan\left[262.5(\varepsilon_s - 0.2)\right]}{\pi} \tag{25}$$

When two or more additional dispersed phases are modeled an additional drag coefficient has to be calculated between those phases. This has been accomplished by applying interphase symmetrical drag coefficient initially proposed by Syamlal et al. [**?**] and defined as

$$K_{\text{sym},qs} = \frac{3(1+e_{qs})\left(\frac{\pi}{2} + C_{\text{fric},qs}\frac{\pi^2}{8}\varepsilon_s\rho_s\varepsilon_q\rho_q\left(d_q + d_s\right)^2 g_{0,qs}\right)}{2\pi\left(\rho_q d_q^3 + \rho_s d_s^3\right)}\left|\mathbf{u}_q - \mathbf{u}_s\right| \tag{26}$$

where q denotes additional dispersed phase, e_{qs} is the coefficient of restitution, $C_{\text{fric},qs}$ defines the friction between the qth and sth solid phase particles and $g_{0,qs}$ is the radial distribution function.

In the standard DDEM approach where the KTGF is used to model interactions between particles the granular temperature that describes collision in solid phase needs the be calculated.
The granular temperature is described as the mean square value of the random particle velocity fluctuations about the mean flow velocity [17] and can be seen as a kind of turbulent kinetic energy or energy of the solid velocity fluctuations. This quantity cannot be explicitly measured as no granular temperature thermometer is known. An exhaustive overview of various aspects of granular temperature can be found in the review paper [41]. The granular temperature Θ in the constitutive equations for the granular pressure, viscosity and drag force represents thus the particles velocity fluctuation C

$$\Theta = \frac{1}{3}\left\langle C_x^2 + C_y^2 + C_z^2\right\rangle \tag{27}$$

The granular temperature defined for each solid phase s is governed by the following transport equation

$$\frac{3}{2}\left[\frac{\partial}{\partial t}(\varepsilon_s\rho_s\Theta) + \nabla\cdot(\varepsilon_s\rho_s\Theta\mathbf{u}_s)\right] = \nabla\cdot(k_\Theta\nabla\Theta) - \nabla p_s + \tau_s : \nabla\mathbf{u}_s - \gamma_s + \varphi_{fs} \tag{28}$$

where γ_s is a dissipative term which represents the rate of energy dissipation within the solid phase due to collisions between particles, $\tau_s : \nabla\mathbf{u}_s$ represents the fluctuating energy caused by the forces acting between particles (viscous dissipation), $\nabla\cdot(k_\Theta\nabla\Theta)$ stands for the diffusion, φ_{fs} is the exchange term which represents

the kinetic energy transfer between phases [20], k_Θ is the conductivity of the granular temperature and p_s is the granular pressure. Due to a high instability of Eq. (28) it is typically replaced by an algebraic formulation described in [42] and [20]. The algebraic equation for granular temperature has been derived based on the assumption that the granular kinetic energy does not change significantly in time and is dissipated locally, hence the terms representing the convection and diffusion can be neglected [43, 20]. The differential equation for the granular temperature is then simplified to

$$-\nabla p_s + \tau_s : \nabla \mathbf{u}_s - \gamma_s + \varphi_{fs} = 0 \tag{29}$$

The energy dissipation due to particle collisions γ_s is usually calculated using expression proposed by Lun at al. [37]

$$\gamma_s = \frac{12(1-e_{ss}^2)g_{0,ss}}{\bar{d}_s\sqrt{\pi}}\rho_s\Theta^{3/2}\varepsilon_s^2 \tag{30}$$

where $g_{0,ss}$ is the radial distribution function, $\bar{d}_s$ is the aveage particle size in given numerical cell. When the restitution coefficient e_{ss} in Eq. (30) tends to unity, the dissipation of kinetic energy within the solid phase becomes negligible $\gamma_s \to 0$.

3.2. Discrete Element Method

For accurate prediction of interaction between particles and particles with fluid as well as Particle Size Distribution (PSD) Discrete Element Method can be used. DEM approach defines collisions using two models: soft-sphere and hard-sphere. In this, based on the work of Cundall and Stack [44] implemented in ANSYS Fluent takes into consideration the spring deformation and shape of particle resulted from collision. Particle motion is described by equation (31) using Newton's second law [45]

$$\frac{\mathrm{d}\mathbf{u}_p}{\mathrm{d}t} = F_\mathrm{D}(\mathbf{u}_f - \mathbf{u}_p) + \frac{\mathbf{g}(\rho_p - \rho_f)}{\rho_p} - \frac{\nabla p}{\rho_p} - F_{coll} \tag{31}$$

$$\frac{dx_p}{dt} = u_p \tag{32}$$

where $\vec{F}_{coll}$ - force resulting from collision of particles. The figure below illustrates in a exaggerated way, the collision effect between two particles. Both of them have different masses m_1 , m_2 and radii r_1, r_2 but forces resulting from collision are the same.

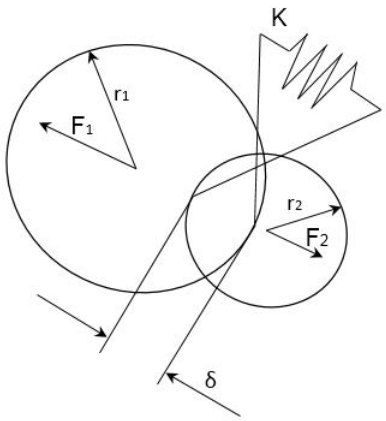

Figure 6: Mapping of particle collisions using the DEM approach (K defines the spring constant, F_1 and F_2 are the forces resulting from collisions)

The linear spring-dashpot collision law was chosen for modeling particle interactions. To determine forces of collisions, the following expressions are used [33]

$$\vec{e}_{12} = \frac{x_2 - x_1}{||x_2 - x_1||} \tag{33}$$

$$\delta = ||x_2 - x_1|| - (r_1 + r_2) \tag{34}$$

where $\vec{e}_{12}$ is a unit vector, x_1 and x_2 are positions of particle centers. Also including the coefficient of restitution into collision the following expressions have to be evaluated [33]

$$f_{loss} = \sqrt{\pi^2 + ln^2\eta} \tag{35}$$

$$m_{12} = \frac{m_1 m_2}{m_1 + m_2} \tag{36}$$

$$t_{coll} = f_{loss}\sqrt{\frac{m_{12}}{K}} \tag{37}$$

$$\gamma = -2\frac{m_{12} ln\eta}{t_{coll}} \tag{38}$$

$$\vec{v}_{12} = \vec{v}_2 - \vec{v}_1 \tag{39}$$

where f_{loss} - loss factor, m_{12} - reduced mass, t_{coll} - collision time, η coefficient of restitution for the dashpot term, $\vec{v}_1$ and $\vec{v}_2$ - velocities of particles, $\vec{v}_{12}$ - relative velocity between particles, γ is a damping coefficient. Going through previous expressions the force F_1 is calculated as [33]

$$\vec{F}_1 = (K\delta + \gamma(\vec{v}_{12}\vec{e}_{12}))\vec{e}_{12} \tag{40}$$

where K is a spring constant. According to Newton's second law, knowing the value of $\vec{F}_1$, $\vec{F}_2$ can be determined

$$\vec{F}_2 = -\vec{F}_1 \tag{41}$$

The DEM model is dedicated for simulating single particle motion. However, in many cases (as fluidization in CFB units, cereal in a silo) the number of particles is large and computational resources are limited. In order to overcome this problem and decrease the required computational power particle are packed in parcels, according to equation

$$NP = \frac{\dot{m}_{parcel}\Delta t}{m_p} \tag{42}$$

where NP - number of particle in parcel, $\dot{m}_{parcel}$ - mass flow of parcel, Δt - time step and m_p - particle mass.

3.3. Heat transfer for single particle

Analyzing multiphase flow one- and two way coupling between phases come into play [4]. In one-way coupling, fluid influences particle movement but there is no backward effect from particle motion on the fluid. In two-way coupling both fluid and particles influence one another. The coupling between phases even increases importance while considering heat transfer taking place between phases. For better understanding figure 7 illustrates the described problem. Figure 7a shows one way-coupling when changes in the temperature of the particle do not influence the temperature and the velocity field of the fluid. When two-way coupling is taken into account, the heat transfer between solid and fluid phase influences both temperature and velocity field (see Fig. 7b). Two way-coupling cannot be omitted, when considering combustion processes.

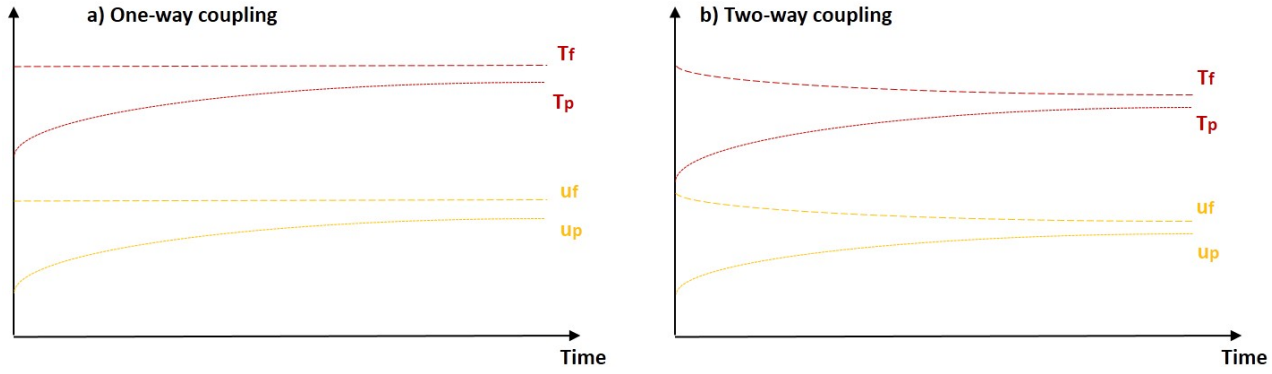

Figure 7: Illustration of one-way and two-way coupling during particle heating [4]

To simulate heat and mass transfer process during combustion of solid fuel, the heating, evaporation, devolatilization and oxidation processes need to be accounted for. To simulate numerically combustion process of coal particles several assumptions have to be introduced:

- the particle temperature is uniform,
- the coal particle is composed of ash, moisture, volatile and char,
- ash is treated as an inert material,
- the coal particles are spherical and have homogeneous physical and chemical properties,
- different processes cannot take place simultaneously, one of the process has to be finished to occur the next one,
- char combustion starts once all the volatile matters have evolved, however in reality they can overlap,

- the composition of volatiles which contain hydrocarbon, nitrogen, oxygen, sulfur, carbon is defined as an input for the devolatilization reaction,
- moisture loss is controlled by heat transfer to the particle and vapor diffusion form coal particle to the gaseous phase.

When the heat and combustion process is taken in to account, the variation of mass and temperature of the particles have to be taken into account. This is accounted for by solving particle mass and energy balance equations.

3.4. Combustion process

Combustion is a rapid chemical process of oxidizing, releasing great amount of heat. Substrates of combustion are substances supplied to the domain (fuel and air) while products are substances released (flue gas, gaseous and solid substances) [46]. The solid fuel combustion process consists of few steps: heating, evaporation, devolatization, oxidation. A simple scheme of this process is illustrated in Fig. 8. In the first stage of the combustion process the injected particle is heated up to a defined evaporation temperature. Over the evaporation temperature the evaporation process proceeds until moisture is removed from the particle. After evaporation the particle is again heated to devolatilization temperature, above which the gaseous fraction is released from the particle to the continuous phase, where the volatile matters are combusted. After devolatilization, the char combustion process starts. When the entire char in the particle is consumed, the heating process is again activated and remaining hot ash is used as the inert material for heat transfer processes.

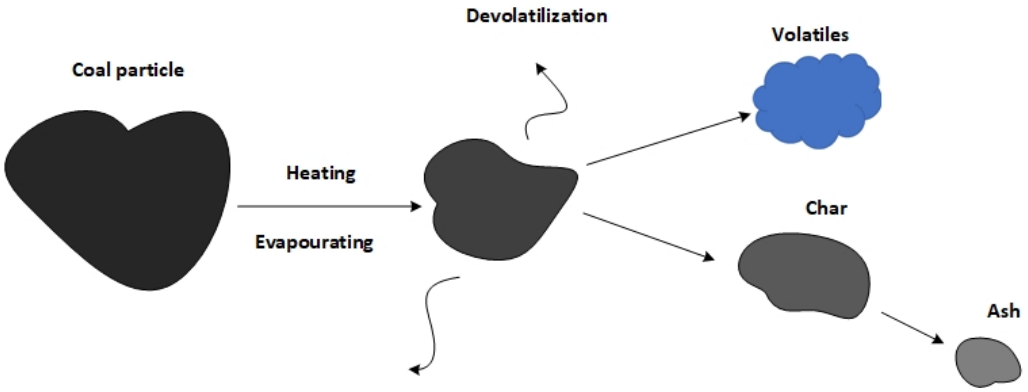

Figure 8: Scheme of coal particle conversion

During combustion of the coal particle, its mass and temperature are changing. Therefore mass and energy equations have to be solved. The mass change of the coal particle is described by following equation

$$\frac{\mathrm{d}m_p}{\mathrm{d}t} = \frac{\mathrm{d}m_{\mathrm{char}}}{\mathrm{d}t} + \frac{\mathrm{d}m_{\mathrm{vol}}}{\mathrm{d}t} + \frac{\mathrm{d}m_{\mathrm{w}}}{\mathrm{d}t} \tag{43}$$

where m_{char}, m_{vol} and m_{w} are the mass of the char, volatiles and water in the combustible particle respectively. During combustion the amount of ash material in the coal particle remains constant. The heat transfer between the surrounding gases and particle can be described by solving the particle energy balance equation, which is written as

$$m_p c_p \frac{\mathrm{d}T_p}{\mathrm{d}t} = A_{\mathrm{ext}} h \left(T_f - T_p\right) + Q_c \tag{44}$$

where c_p and T_p stands for the particles specific heat and temperature, h is the heat transfer coefficient to particle calculated using the correlation of Ranz and Marshall on the Nusselt number, A_{ext} represents the particle

surface area, Q_c stands for the changes of energy due to the evaporation and surface combustion processes.

As mentioned in the beginning of this chapter coal combustion consists of four stages. The combustion process starts from heating and evaporation processes. When surrounding gas has higher temperature than particle, heating occurs according to equation (44), excluding part responsible for energy absorbed for evaporating moisture from particle. Fuels differs in moisture content, it varies; for hard coal from 3 to 10%; for lignite from 10 to 50% and for biomass from 5 to 70% [47]. Evaporation involves changing the mass of the particle, which is expressed by the formula

$$\frac{\mathrm{d}m_w}{\mathrm{d}t} = -N_{\mathrm{H_2O}} A_{\mathrm{ext}} M_{\mathrm{H_2O}} \tag{45}$$

where $M_{\mathrm{H_2O}}$ - molar mass weight of water vapour, $N_{\mathrm{H_2O}}$ - molar flux of water vapour expressed as

$$N_{\mathrm{H_2O}} = k_c \left(C_{\mathrm{H_2O},p} - C_{\mathrm{H_2O},f}\right) \tag{46}$$

where $C_{\mathrm{H_2O},p}$ and $C_{\mathrm{H_2O},f}$ - concentration of vapour on the particle surface and in the bulk gas respectively, k_c - mass transfer coefficient, determined from the following equation defining the Sherwood number [48]

$$\mathrm{Sh} = \frac{k_c d_p}{D_{\mathrm{H_2O},m}} = 2.0 + 0.6\mathrm{Re}^{0.5}\mathrm{Sc}^{0.33} \tag{47}$$

where $D_{\mathrm{H_2O},m}$ - diffusion coefficient, Sc - the Schmidt number. The concentration of water vapour on the particle surface and in the core of the gas are calculated as

$$C_{\mathrm{H_2O},p} = \frac{p_{\mathrm{sat}}(T_p)}{RT_p} \tag{48}$$

$$C_{\mathrm{H_2O},f} = X_{\mathrm{H_2O}} \frac{p}{RT_f} \tag{49}$$

where p_{sat} - saturation pressure for specified T_p, R - universal gas constant ($8.314 \frac{kJ}{kmolK}$), $X_{\mathrm{H_2O}}$ - mole fraction of water vapour, p - absolute pressure. The amount of energy absorbed for evaporating water from the particle is calculated as

$$Q_c = \frac{\mathrm{d}m_p}{\mathrm{d}t} h_{\mathrm{fg}} \tag{50}$$

where h_{fg} - entalphy of evaporation

$$h_{\mathrm{fg}}(T_p) = h_{\mathrm{bp}} + \int_{T_p}^{T_{p,\mathrm{bp}}} c_{\mathrm{w}} \mathrm{d}T - \int_{T_p}^{T_{p,\mathrm{bp}}} c_{\mathrm{g}} \mathrm{d}T \tag{51}$$

where lower index *bp* refers to boiling point (373.15K) so $\mathrm{h_{bp}}$ - the entalphy at boiling point, c_{w} and c_{g} - specific heat of water and water vapour.

Devolatilization is an important part of the combustion of coal. The volatile gases burn much more rapidly than the remaining char particles and therefore they are important for flame ignition and stability [49]. Volatile matter (consisting of tar, light gases and water from pyrolysis) is released into continuous phase. Using Badzioch and Hawksley model [50] for describing particle mass changing during devolatization

$$\frac{\mathrm{d}m_{vol}}{\mathrm{d}t} = -k \underbrace{\left[(1 - Y_{\mathrm{char},0} - Y_{\mathrm{w},0} - Y_{\mathrm{ash},0}) m_{p,0}\right]}_{\mathrm{m_{vol,0}}} \tag{52}$$

where k - kinetic rate; $Y_{\mathrm{char},0}$, $Y_{\mathrm{w},0}$, $Y_{\mathrm{ash},0}$ - mass fraction of char, water, ash respectively; $m_{p,0}$ - initial mass of particle, $m_{\mathrm{vol},0}$ - initial mass of volatiles. The kinetic rate is determined from the formula

$$k = A_1 \exp\left(-\frac{E}{RT_p}\right) \tag{53}$$

where A_1 - pro-exponential constant, E - activation energy.

The most dominant process during combustion of a coal particle is the burning of coke breeze. Despite many available advanced models, they are not widely used due to high computational time and complications in obtaining appropriate results. The oxidizing reaction on a particle surface is expressed as

$$\mathrm{C(s)} + \mathrm{O_2} \rightarrow \mathrm{CO_2} \tag{54}$$

The model of Baum and Street [51] describing the diffusion of oxidant on a particle surface, while carbon consumption particle surface stays unchanged, the mass loss is evaluated as:

$$\frac{\mathrm{d}m_{char}}{\mathrm{d}t} = -4\pi d_p D_{\mathrm{O_2},m} \frac{Y_{\mathrm{O_2}} T_f \rho_f}{S_b \left(T_p + T_f\right)} \tag{55}$$

Chemical composition of solid fuels is a sum of gram share of particular compounds [46]

$$c + h + s + o + n + m + a = 1 \tag{56}$$

where c - carbon, h - hydrogen, s - sulfur, o - oxygen, n - nitrogen, m - moisture, a - ash.

$$\left.\begin{aligned} n'_C = \frac{1}{12}c \quad n'_S = \frac{1}{32}s \quad n'_{H_2} = \frac{1}{2}h \\ n'_{N_2} = \frac{1}{28}n \quad n'_{O_2} = \frac{1}{32}o \quad n'_{H_2O} = \frac{1}{18}m \end{aligned}\right\} \tag{57}$$

Above equations express the amount of kilomoles of an element per 1 kilogram of crude fuel.
The oxygen included in fuel [46]:

$$n_{o2min} = \frac{c}{12} + \frac{s}{32} + \frac{h}{4} - \frac{o}{32}, \frac{kmol}{kgfuel} \tag{58}$$

$$n_{amin} = \frac{n_{o2min}}{0.21}, \frac{kmolO_2}{kgfuel} \tag{59}$$

n_{amin} - minimal theoretical amount of air needed for combustion. The real amount of air, is calculated as follows

$$n'_a = \lambda n_{amin}, \frac{kmola}{kgfuel} \tag{60}$$

λ - excess air ratio. The following equations represents the number of kilomoles of substances per per unit of burnt fuel

$$\left.\begin{aligned} n"_{CO2} = n'_C, \quad n"_{SO2} = n'_S, \quad n"_{N2} = n'_{N2} + 0.79n'_a \\ n"_{O2} = 0.21(\lambda - 1)n_{o2min}, \quad n"_{H2O} = n'_{H2} + n'_{H2O} \end{aligned}\right\} \tag{61}$$

The total number of kilomoles of flue gas per unit of burnt fuel is given by

$$n"_{fg} = n"_{CO2} + n"_{SO2} + n"_{N2} + n"_{O2} + n"_{H2O}, \frac{kmolfg}{kgfuel} \tag{62}$$

The products of complete combustion are CO_2, O_2, N_2, SO_2, H_2O and their molar fractions are calculated as follows

$$\left.\begin{aligned}(CO_2) = \frac{n"_{CO2}}{n"_{fg}}, \quad (O_2) = \frac{n"_{O2}}{n"_{fg}}, \quad (N_2) = \frac{n"_{N2}}{n"_{fg}},\\ (SO_2) = \frac{n"_{SO2}}{n"_{fg}}, \quad (H_2O) = \frac{n"_{H_2O}}{n"_{fg}},\end{aligned}\right\} \tag{63}$$

4. Numerical simulations using simplified geometrical models

Geometry and a mesh of simplified combustion chamber were made in Ansys environment. Used geometry is depicted in Fig. 9. Geometry consists of 4,718 hexahedral elements with size of 0.03 m. The dimensions of a domain are $0.2x0.3x2$ m. Solid material is injected through the port located at the left side of the computational domain, 0.15 m above the bottom air inlet, see (Fig. 10). For modeling coal combustion the solid material injection ports have been slightly reconfigured as it can be seen in Fig. 11b. Coal injection ports have been located at the side walls. This operation was done in order to ensure better mixing of the fuel and inert material at the bottom section of the combustion chamber.

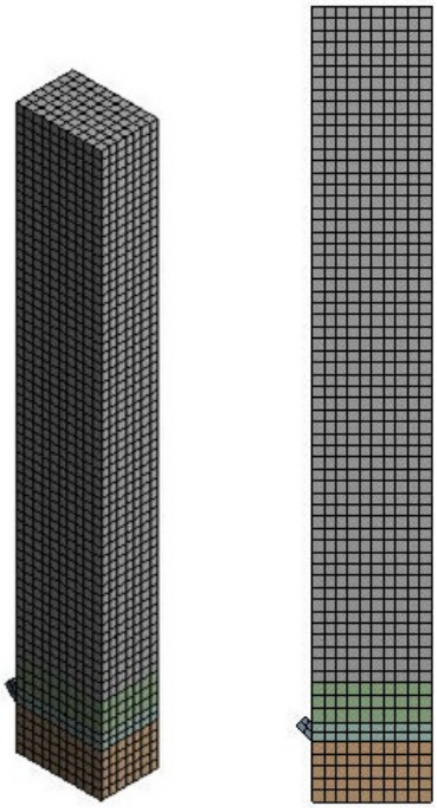

Figure 9: Geometry used for heat transfer modeling

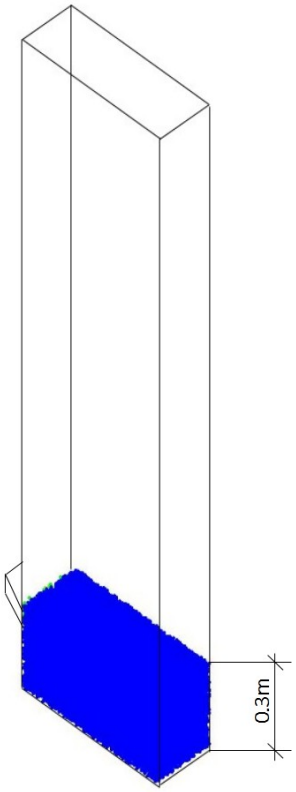

Figure 10: Part of a domain used for injecting sand particles

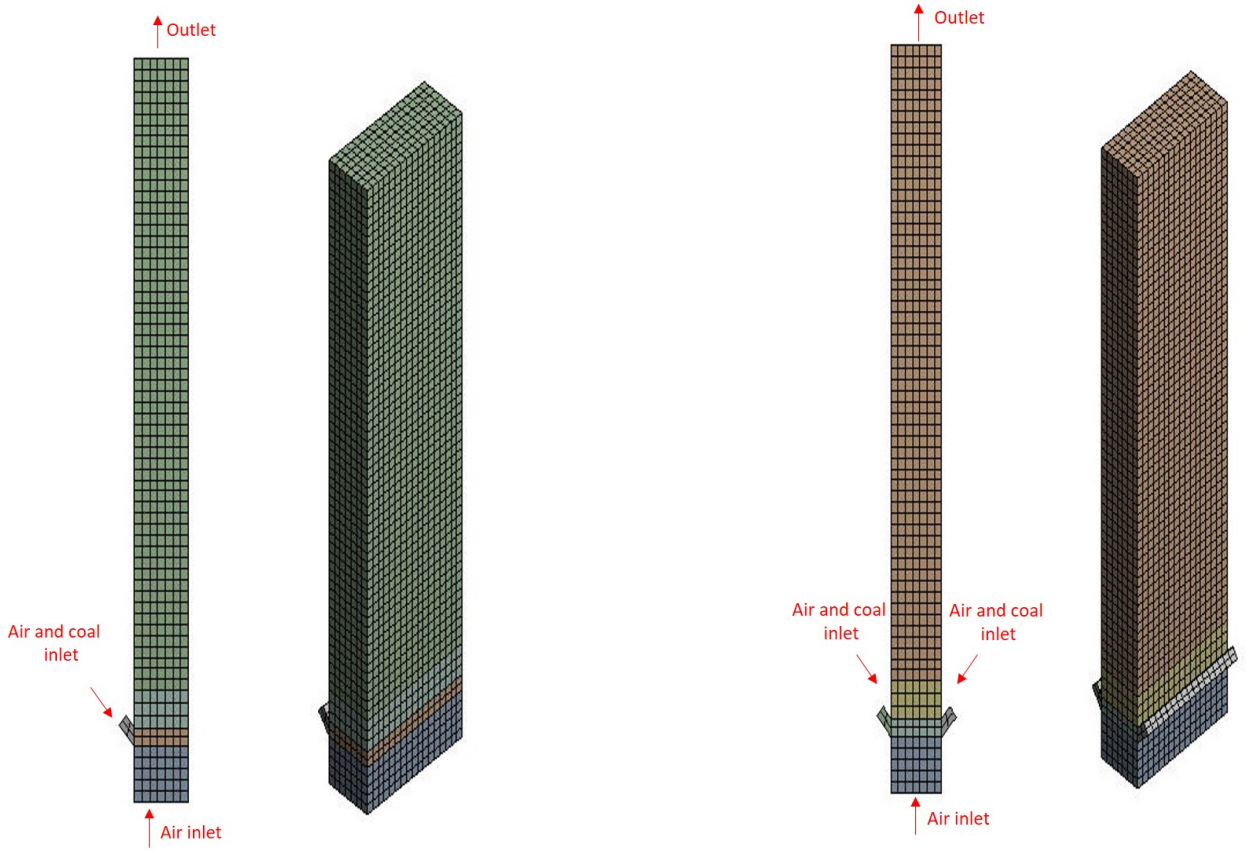

(a) Port of fuel on one side of the domain

(b) Ports of fuel on both sides of the domain

Figure 11: Geometries used for combustion modeling

The calculations were initialized by providing 100,000 particle parcels (named sand) into the bottom part of the geometry. This part of the model is highlighted in Fig. 10. In order to initialize the simulation using predefined amount of material within computational domain the built-in Ansys Fluent feature was used. Using the volume injection method it is possible to prescribe defined amount of material to the selected zones of the model. The initial velocity of the sand was set to zero. In case of modeling only mixing with heat transfer the initial sand temperature was set to 383 K while modeling combustion the initial sand temperature was set to 1173 K. At the walls a no slip condition was assigned. The restitution coefficient between particles and wall collisions was set to 0.9. At the outlet the pressure outlet boundary condition was assigned with a gauge pressure equals to 0.

As it was mentioned earlier effect of modeling only the heat transfer process between gaseous and solid phases also the parcel mixing process was investigated. This was organized by injecting solid material (named here as coal) through the port located at the side ports of the computational domain. For heating purpose the hot air was provided to the domain through bottom inlet with temperature equal to 573 K. The properties of the injected materials are listed in table 1.

Table 1: Input parameters for heat transfer

Material	**Parameter**	**Value**	**Unit**
Sand	Number of parcels	100,000	-
	Diameter of particles	500	μm
	Initial temperature of parcels	383.15	K
	Density	2400	kg/m3
Coal	Diameter of particles	125	μm
	Initial temperature of parcels	383.15	K
	Density	1200	kg/m3
Air	Velocity through side inlet	6.63	m/s
	Velocity from the bottom	2.65	m/s
	Temperature through side inlet	1173.15	K
	Temperature from the bottom	1173.15	K

The input parameters for air and fuel supplied to the domain for combustion case are collected in table 2. The composition of the coal is shown in table 3. The value of the Lower Heating Value of coal was 11/400 $\frac{\text{kJ}}{\text{kg}}$.

Table 2: Input parameters.

		1 side inlet	2 side inlet	Unit
Particle diameter		125	125	μm
			300	μm
Fuel mass flow		0.022		kg/s
Air mass flow	inlet_{side}	0.010		kg/s
	inlet_{bottom}	0.093		kg/s
Air temperature	inlet_{side}	413.15		K
	inlet_{bottom}	593.15		K

Table 3: Ultimate and proximate analysis of burnt coal

Proximate, %		Ultimate, %	
Ash	10.80	C	30.38
Water	46.80	H	2.46
VOL	23.51	S	0.38
Char	18.89	N	0.31
		O	8.87

The air has been modeled as an incompressible ideal gas. The simulation time was set to three seconds while the time step was set to 0.001s. The effect of heat transfer between gaseous and solid phases was resolved in terms of the convection and conduction. The radiation was not taken into account due to high loads of solid material within the domain. In order to ensure good stability of the solution procedure, appropriate selection of the discretization schemes for transport equation needs to be done. In discussed case the quadratic interpolation scheme was used for discretization of the continuity equation, while for the momentum equations a second order discretization schemes was used for the convective terms. For the energy equation the first-order upwind discretization scheme was used. Additionally, during combustion modeling, it was important to monitor flow parameters, i.e. composition of the flue gas, temperature, and amount of unburnt coal at the outlet from the

domain.

To check the energy conservation, a global energy balance needs to be carried out. For that purpose the following relations was used

$$E_{in} = \Delta E_u + E_{out} \tag{64}$$

where E_{in} - energy supplied to the system, ΔE_u - increase of internal energy of the system, E_{out} - energy derived from the system. The above equation in a detail takes form:

$$E_{chfuel} + E_{pfuel} + \Sigma E_{air_{1,2}} + E_{sand_{T0}} = E_{sand_{T1}} + \Sigma E_{fg} + E_{pchar} + E_{pash} \tag{65}$$

where E_{chfuel} - chemical energy of fuel, E_{pfuel} - sensible entalphy of fuel, $\Sigma E_{air_{1,2}}$ - sensible entalphy of air both from side port(s) and bottom of a domain, $E_{sand_{T0}}$ and $E_{sand_{T0}}$ - energy of sand at the beginning of simulations and at the end respectively, ΣE_{fg} - energy of flue gasses, E_{char} - energy of char, E_{ash} - energy of ash.

It should be highlighted here that without information about the amount of unburned coal removed from domain through the outlet the energy balance cannot be closed. Therefore user defined function (UDF) for collecting necessary data, i.e. mass of char, mass of ash were developed and implemented into the solution procedure. The main objective was to collect the mass of char and ash at the outlet for calculating the energy leaving through the outlet.

4.1. Results

A set of numerical calculations has been carried out for two configuration. The results have been divided between heat transfer and mixing processes and combustion. Firstly the heat transfer between gaseous and solid phases was investigated together with mixing of the solid material. In the second stage the combustion of coal together with mixing of sand has been taken into account. Subsequent results have been illustrated using the contours of solid volume fraction using logarithmic scale and temperature of solid phase, parcels distribution colored by solid phase temperature. The changes of physical property of mentioned variables were illustrated after 0.01 s, 1.5 s and 3 s from beginning of simulation.

As it was mentioned, the results will be discussed starting from heat transfer and mixing processes. In Fig. 13 it can be seen that during the simulation the solid volume fraction located in the injection zone gradually decreases. This is caused by fluidization air provided through the bottom of the domain. After the material reaches the minimal fluidization velocity (4.5 m/s) particle starts to move upwards the free surface between solid and gas. When particles velocity reached terminal velocity particles are entrained by the gas. Finally the turbulent mixing occur where particles almost uniformly cover computational domain. As it can be seen in Fig. 15 the temperature of the sand increased by approximately 10 K globally. The simulation time was only 3 s, it was not enough to ensure uniform temperature distribution over the solid phase. It should be also pointed out that the heat transfer process modeled by applying the DEM approach used the properties of parcels. To prove this simple analytical calculations for single parcel and particle were carried out. The equation used for that purpose assumes the form [4]:

$$\frac{dT_d}{dt} = \frac{Nu}{2}\frac{1}{\tau_t}(T_c - T_d) \tag{66}$$

where Nu - Nusselt number, τ_t - particle response time, calculated as follows [4]:

$$\tau_t = \frac{\rho_p c_p d_p^2}{12 k_f'} \tag{67}$$

where c_p - heat capacity of particle, $12k'_f$ - thermal conductivity of fluid.

To determine curve of temperature change in time for the parcel with diameter of 4 mm, first response time was determined using equation (67). Then using equation (66) the temperature at every time step was calculated. This procedure was repeated also for a possibility if the parcel had the same diameter as particle (which is 500 μm). The response time for a parcel is 222.2 s and for particle is 3.47 s. It means that after this particular time parcel would reached the temperature of surrounding gas. Calculation results covers the simulation outcome. The parcels increased its temperature of 10.56 K in 3 s, if parcels would have the same diameter as particles after 3 s of simulations their temperature would reach almost the same value. To draw the conclusions from simulations heat transfer is calculated not for a single particle but for the parcel. For the best prediction parcel would have to contain only one particle so parcel would have the same diameter.

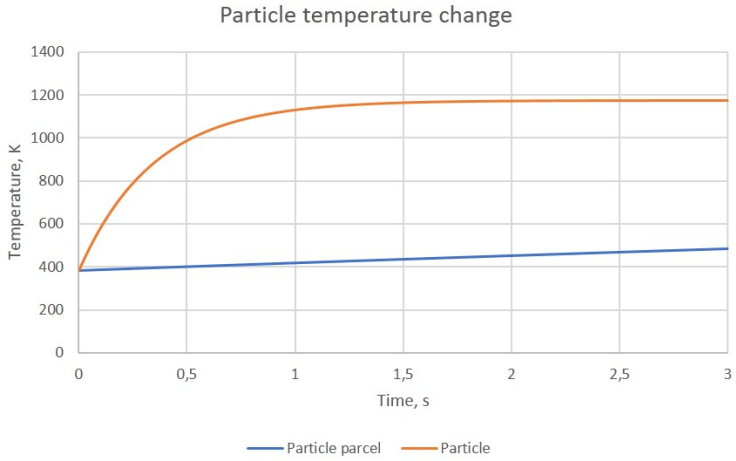

Figure 12: Particle temperature change in time

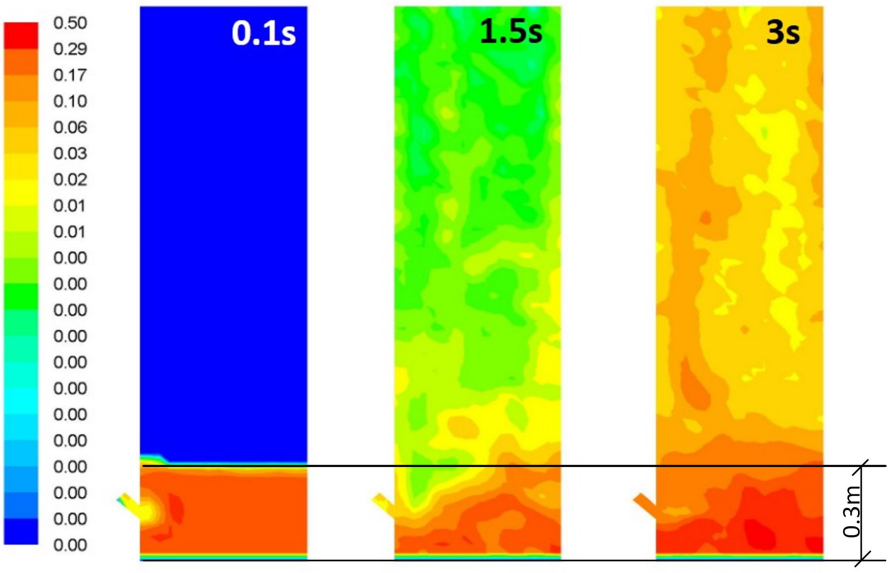

Figure 13: Volume fraction of solid phase in 0.1s, 1.5s and 3s of simulation respectively

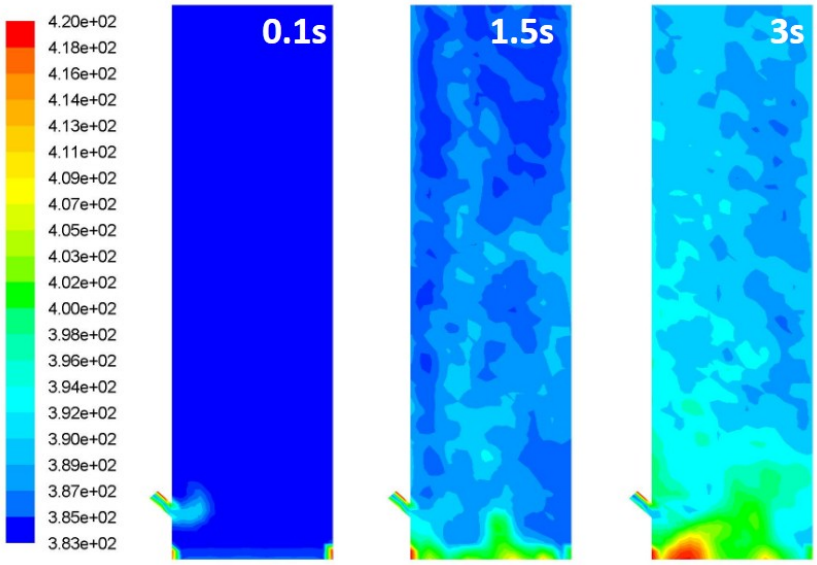

Figure 14: Temperature of solid phase in 0.1s, 1.5s and 3s of simulation respectively

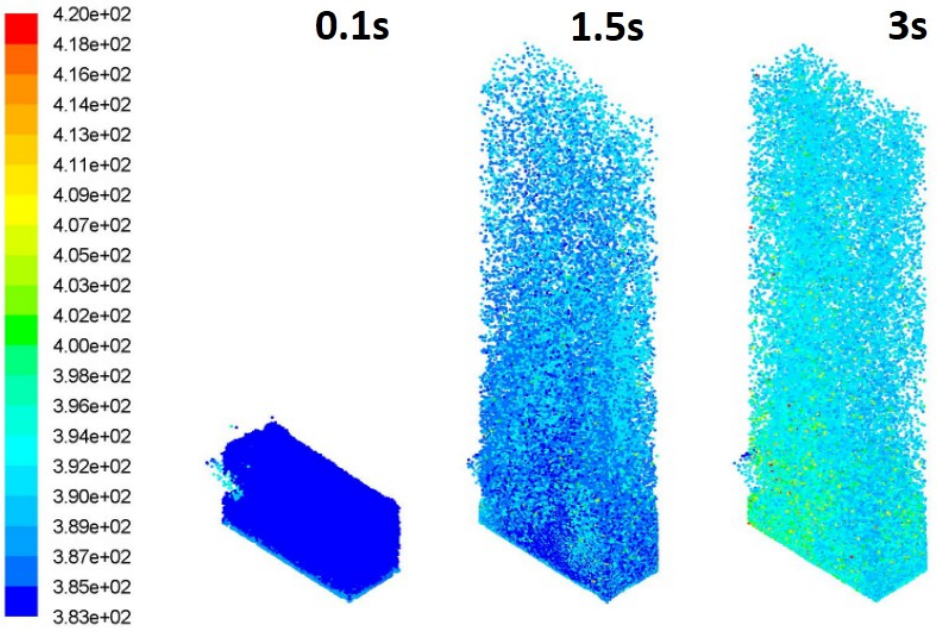

Figure 15: Particle temperature in 0.1s, 1.5s and 3s of simulation respectively

The combustion process is discussed based on the contours of the solid phase temperature shown in Fig. 17 and contours of CO_2 mass fraction depicted in Fig. 19. Additionally to visualize the particle transport parcels distribution colored by temperature of the inert material has been used. Particle distribution is shown in Fig. 20. All instantaneous results have been collected after 0.1 s, 1.5 s and 3 s of the simulation.

The combustion chamber was assumed to be adiabatic, which means it does not exchange heat through the walls, so the whole energy is absorbed and accumulated by the inert material. Initial values of CO_2, H_2, O_2 were set as 0.1, of a N_2 as 0.6 and the initial temperature was 1173 K.

Figures 17, 18 illustrates the instantaneous temperature distribution for two configuration of the coal injection ports of the solid and gaseous phases, respectively. It can be seen that for case with two inlets the temperature distribution at the bottom section of the rig is quite uniform. The fludization gases affect the distribution of the solid material in the riser which affect the temperature distribution in the upper section of the riser. Figure 17 shows that in the zones where lower volume fraction of solid phases exist high non uniformity in temperature distribution can be expected. The effect of non uniform distribution of solid material within the riser for both of the considered cases can be seen in Fig. 20 where small fraction of solid material is entrained by passing gas. This is casused by the properties of the inert material which is quite heavy and parcels are relatively large. High temperature next to the combustion chamber walls at the beginning of simulations is caused by defined temperature at boundary equal to 1173 K. However, this effect vanished during simulation due to exchange heat between walls, gas and particles. Mass fraction of flue gas as well as temperature stabilize faster (after approximately one second of simulations) when two ports supplying oxidizer and fuel are present which can be seen in Fig. 16 where the fluctuations of selected parameters changing over time at the outlet from the riser are presented. This data has been collected using user defined function implemented into the solution procedure. It can be seen that for the case with one injection ports, even at the end of simulation the carbon-dioxide distribution did not approach uniformity. Nevertheless, this solution is more stable in contrary

to the data collected for single solid injection port.

Based on the carried out set on numerical simulations it can be clearly seen that for the geometry configuration which consists two injection ports located at the both sides of the riser the rate of mixing of the solid material is more intensive in comparison to the case with single injection port. Intensive mixing helps in ensuring the uniform combustion of solid material and distribution of combustion products as well as gaseous phase temperature. The quality of the mixing results in higher temperature inside furnace which can be seen in Fig. 18 as well as CO_2 mass fraction distribution illustrated in Fig. 19. The consequence of bad mixing is local rise of temperature which is not allowed in real application, mainly to protect the CFB boiler from uncontrolled damage. Such undesirable situation can be observed for the case with a single injection port (see Fig.17).

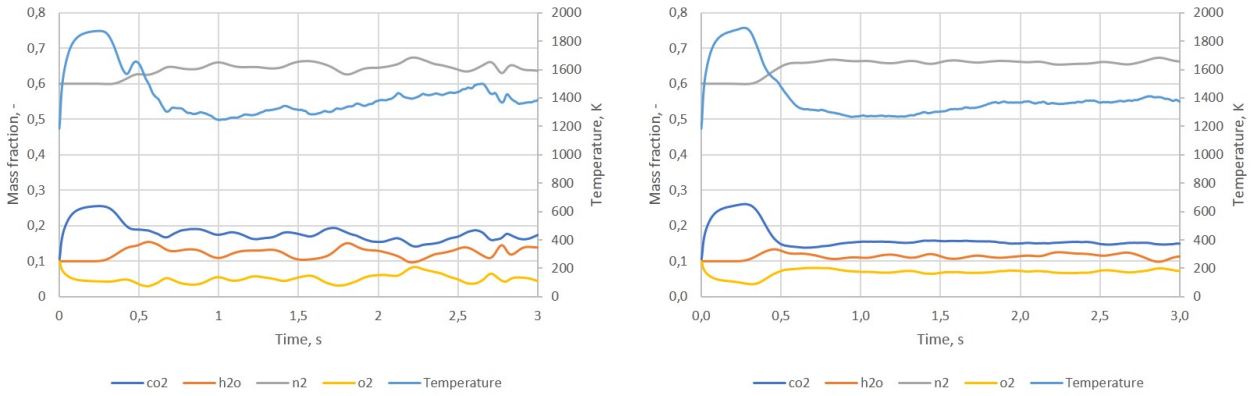

(a) Single injection port located at one side of the riser

(b) Injection ports located at both sides of the riser

Figure 16: Variation of the selected parameters at the outlet form the riser collected during numerical simulations

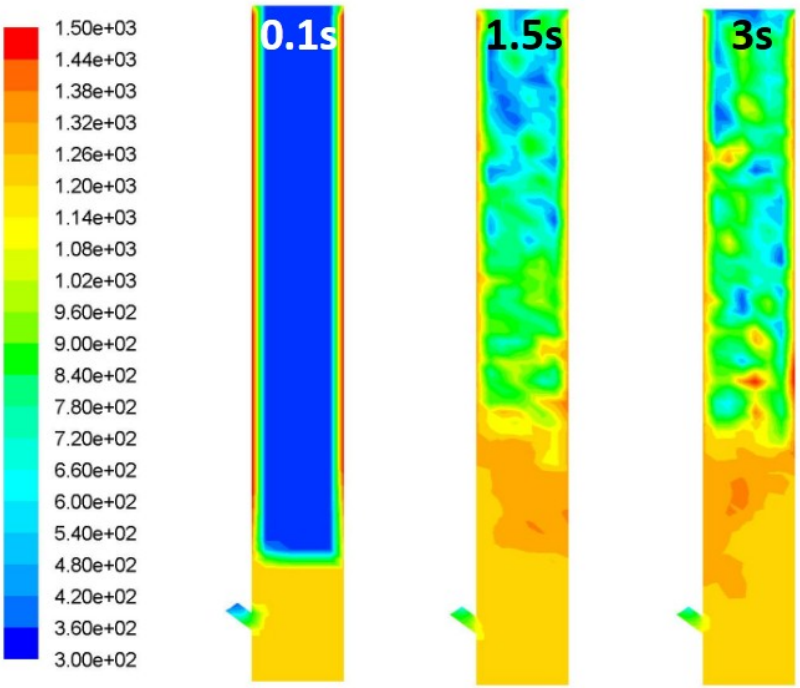

(a) Single solid injection port

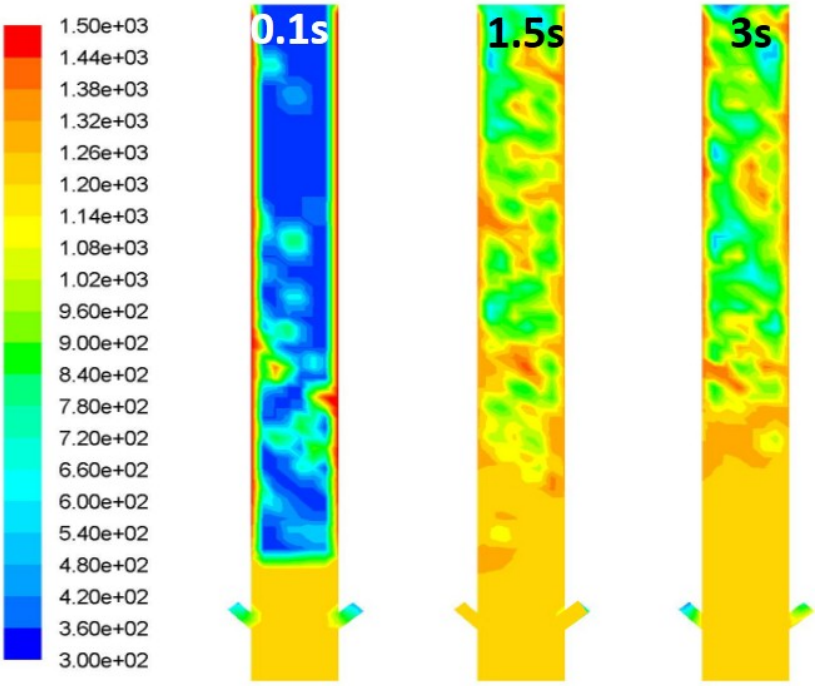

(b) Inlets on both sides

Figure 17: Temperature of solid phase after 0.1s, 1.5s and 3s of numerical simulation

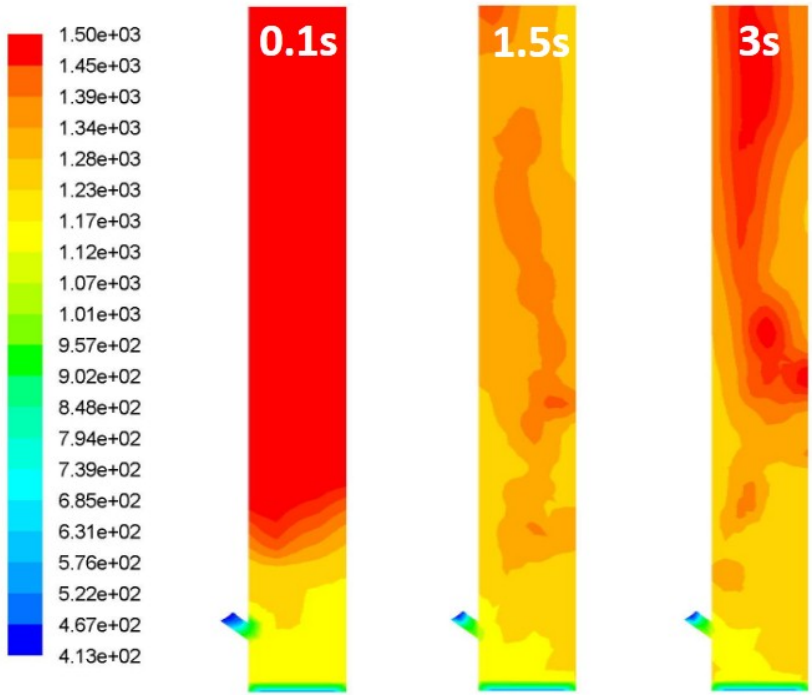

(a) Single solid injection port

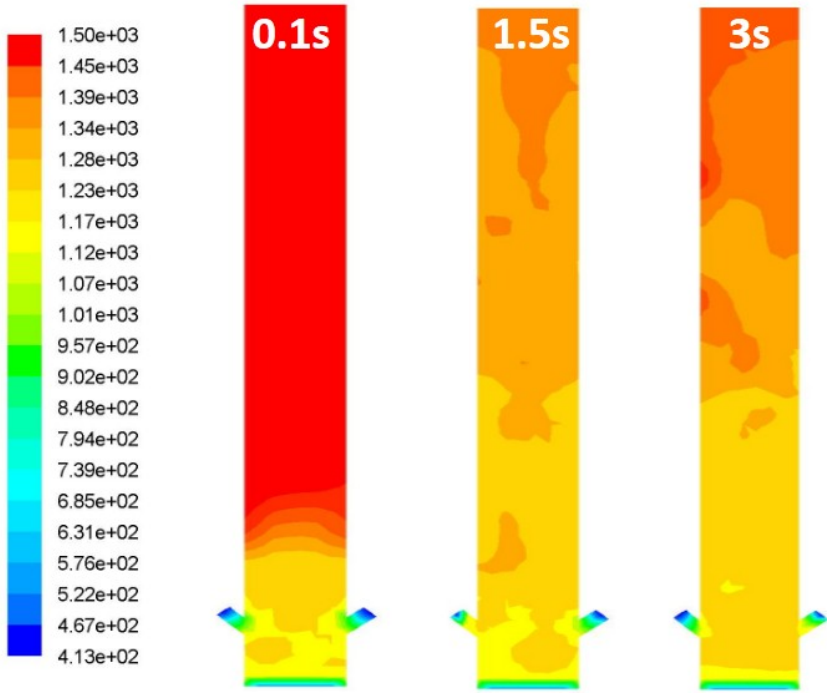

(b) Inlets on both sides

Figure 18: Temperature of gaseous phase after 0.1s, 1.5s and 3s of numerical simulation

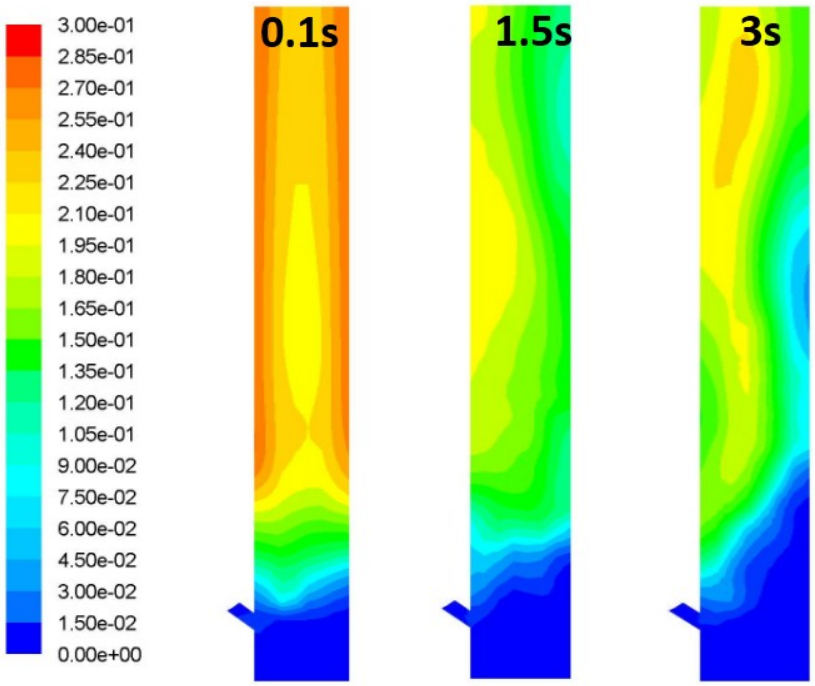

(a) Injection ports located at one side

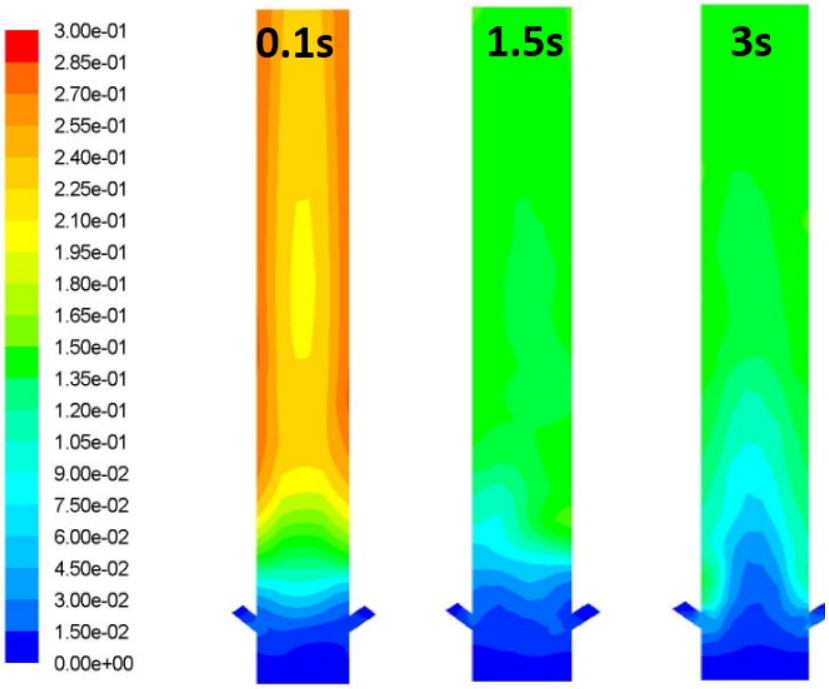

(b) Injection ports located at both sides

Figure 19: Mass fraction of CO_2 after 0.1s, 1.5s and 3s of numerical simulation

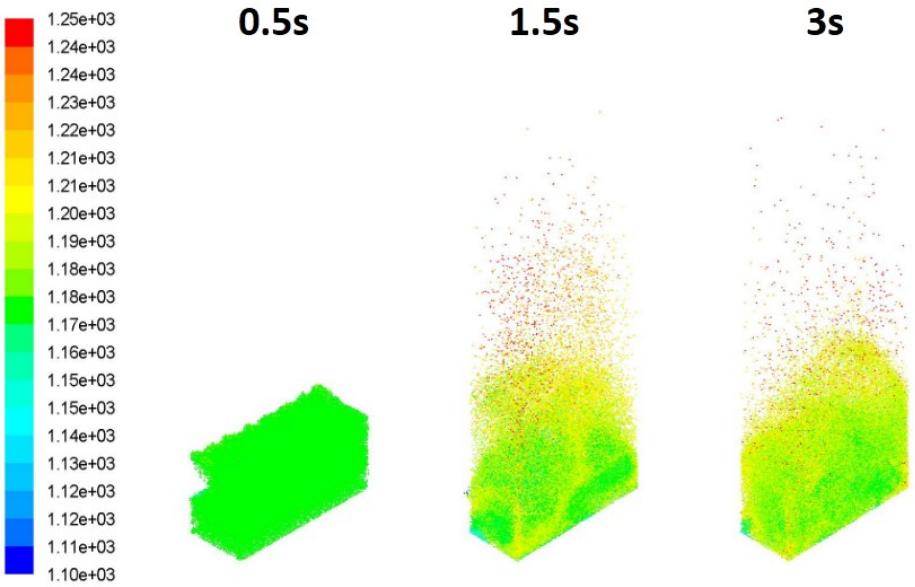

(a) Injection ports located at one side

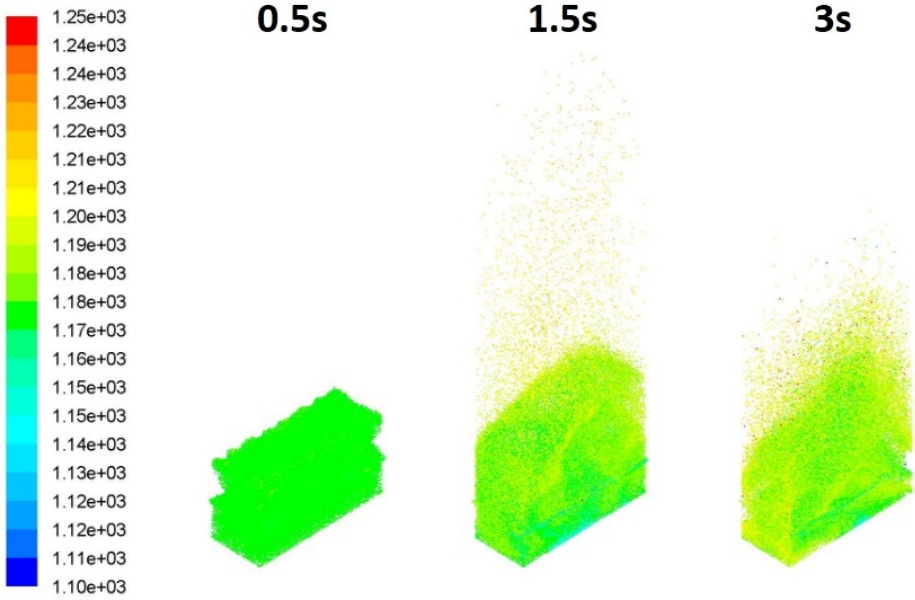

(b) Injection ports located at both sides

Figure 20: Temperature of sand in 0.1s, 1.5s and 3s of simulation respectively

An additional step that was carried out to validate the DEM approach was the comparison of numerically calculated composition of the flue gases with those calculated analytically using the set of equations (57)-(63). For all calculation the same fuel and oxidizer parameters were used. The used fuel composition can be found in

table 3. The set of numerical results were gathered and averaged after the flow was stabilized (three seconds) and collected during next three seconds of simulations. The same procedure was used for both cases. This ensures that during the time averaging process the mass fractions of considered species at the outlet were stable. In analytical calculation it was assumed that the combustion is total and complete, it means that the gaseous products are only CO_2, O_2, N_2, SO_2, and H_2O. Moreover there was no unburnt char within removed inert material. An example of the calculation procedure using analytical equations is presented below. The first step is to calculate the amount of kilomoles of a compound per kilogram of fuel:

$$n'_c = \frac{1}{12}\ 0.3038 = 0.02531\frac{kmolC}{kgfuel} \tag{68}$$

$$n'_S = \frac{1}{12}\ 0.0034 = 0.0001\frac{kmolS}{kgfuel} \tag{69}$$

$$n'_{H_2} = \frac{1}{2}\ 0.0246 = 0.0123\frac{kmolH_2}{kgfuel} \tag{70}$$

$$n'_{N_2} = \frac{1}{28}\ 0.0031 = 0.0001\frac{kmolN_2}{kgfuel} \tag{71}$$

$$n'_{O_2} = \frac{1}{32}\ 0.0887 = 0.0028\frac{kmolO_2}{kgfuel} \tag{72}$$

$$n'_{H_2O} = \frac{1}{18}\ 0.4680 = 0.026\frac{kmolH_2O}{kgfuel} \tag{73}$$

$$n'_{O_2min} = \frac{1}{32}\ 0.0887 = 0.0028\frac{kmolO_2}{kgfuel} \tag{74}$$

Then oxygen included in a fuel is calculated

$$n_{o2min} = \frac{0.3038}{12} + \frac{0.0034}{32} + \frac{0.0246}{4} - \frac{0.0887}{32} = 0.0288\frac{kmolO_2}{kgfuel} \tag{75}$$

The minimal theoretical amount of air needed for complete combustion process is given by

$$n_{amin} = \frac{0.0288}{0.21} = 0.1372\frac{n_{amin}}{kgfuel} \tag{76}$$

The real amount of air needed for burning fuel is calculated as

$$n'_a = 1.292 \cdot 0.1372 = 0.1773\frac{kmola}{kgfuel} \tag{77}$$

The mass of flue gas compounds per kilogram of fuel:

$$n"_{CO_2} = n'_{CO_2} \cdot M_{CO_2} = 1.1141 \cdot 44 = 49.0308\frac{kgC}{kgfuel} \tag{78}$$

$$n"_{O_2} = (\lambda - 1) \cdot M_{O_2} = (1.292 - 1) \cdot 32 = 0.2693\frac{kgO_2}{kgfuel} \tag{79}$$

$$n"_{N_2} = n'_{N_2} + 0.79n'_a \cdot M_{N_2} = (0.0001 + 079 \cdot 0.1773) \cdot 28 = 3.9253\frac{kgN_2}{kgfuel} \tag{80}$$

$$n"_{SO_2} = n'_S \cdot M_S = 0.0001 \cdot 64 = 0.0077 \frac{kgSO_2}{kgfuel} \tag{81}$$

$$n"_{H_2O} = (n'_{H_2O} + n'_{H_2} \cdot M_{H_2O} = (0.0123 + 0.026) \cdot 18 = 0.6903 \frac{kghH_2O}{kgfuel} \tag{82}$$

$$n"_s = (n"_{CO_2} + n"_{O_2} + n"_{N_2} + n"_{SO_2} + n"_{H_2O} = 1.1141 + 0.2693 + 3.9253 + 0.0077 + 0.6903 = 6.0066 \frac{kgfg}{kgfuel} \tag{83}$$

$$n"_{ss} = (n"_{CO_2} + n"_{O_2} + n"_{N_2} + n"_{SO_2} = 1.1141 + 0.2693 + 3.9253 + 0.0077 = 5.3163 \frac{kgdfg}{kgfuel} \tag{84}$$

where lower index fg stands for wet flue gas and dfg stands for dry flue gas. The mass fraction of the compounds in the flue gas is calculated as follows:

$$(CO_2) = \frac{n"_{CO2}}{n"_{fg}} = \frac{1.1140}{6.0066} = 0.1855 \tag{85}$$

$$(O_2) = \frac{n"_{O_2}}{n"_{fg}} = \frac{0.2692}{6.0066} = 0.0448 \tag{86}$$

$$(N_2) = \frac{n"_{O2}}{n"_{fg}} = \frac{3.9252}{6.0066} = 0.6534 \tag{87}$$

$$(SO_2) = \frac{n"_{SO_2}}{n"_{fg}} = \frac{0.0077}{6.0066} = 0.0013 \tag{88}$$

$$(H_2O) = \frac{n"_{H_2O}}{n"_{fg}} = \frac{0.6903}{6.0066} = 0.1149 \tag{89}$$

To make sure that the calculation has been done correctly the sum of compounds should be equal to 1.

$$(CO_2) + (O_2) + (N_2) + (SO_2) + (H_2O) = 1 \tag{90}$$

The composition of flue gases obtained from numerical simulations was monitored in every time step during the solution procedure. To obtain the final value, all gathered data was averaged in the time range where the solution was stabilized. This procedure was done both for the case with single and two solid injection ports. Comparison of the numerical and analytical results is presented in table 4. For both investigated configurations of the numerical model, the calculated flow parameters are similar. Some differences can be observed between numerical and analytical results. This can be caused by incomplete combustion of the coal in the considered riser geometry, which means that particles leaving the domain contain a non zero fraction of unburnt char. In the case of total combustion of char, the composition of flue gases calculated analytically and numerically will agree.

As it was already mentioned, the general idea of the fluidized bed is to transfer heat generated during fuel combustion to an inert material that is used as the heat carrier and exchanges it with the combustion chamber walls. Using data collected during the simulations, presented in table 5 and applying the energy balance equation (65) both solutions have been compared. Energy supplied and derived from the system were calculated. The energy absorbed by the sand was determined as the difference between supplied and removed energies from the system, since no losses to the environment was included. The differences are caused by the amount of unburnt coal removed from the computational domain. For case with two injection ports, thanks to intensive mixing between fuel combustion efficiency can be observed. It should be mentioned here that in real systems such situation cannot take place mainly due to the installed recirculation loop which ensures that the combustible fraction from coal will be totally burned.

Table 4: Mass fraction of flue gas components.

Flue gas components	Analythical results, %	Computational results, %	
		1 inlet	2 inlets
(CO2)	18.55	16.89	15.29
(O2)	4.48	5.34	7.05
(N2)	65.35	64.92	66.12
(SO2)	0.13	0.48	0.08
(H2O)	11.49	12.38	11.47

Table 5: Flue gas parameters and energy balance

	1 inlet	2 inlets	Unit
$T_{outlet} =$	1364.28	1345.02	K
$\dot{m}_{char} =$	4.59E-07	3.06E-07	kg/s
$\dot{m}_{ash} =$	8.33E-07	1.02E-07	
$\dot{m}_{fluegas} =$	0.1229	0.1323	
$E_{in} =$	283.20	283.20	kW
$E_{out} =$	164.26	172.28	
$E_{in} - E_{out} =$	118.95	111.31	

5. Numerical simulations of the laboratory scale test-rig

5.1. Geometrical model

Similarly to the heat transfer modeling, a three-dimensional computational domain and mesh of the experimental rig were made in Ansys environment. The model was created based on the laboratory scale CFB test unit, located at the Lappeenranta University of Technology at Laboratory of Modeling of Energy Systems [32]. The same stand has been already used for modeling fluidization of the solid material using DDPM-HEL approach in [52]. The general scheme of the installation is depicted in Fig (21). The complete test rig, working as a real CFB unit, consists of a riser, loop-seal and drain section. The loop-seal itself is composed of the cyclone (device separating gas and solid particles) and a downcomer.

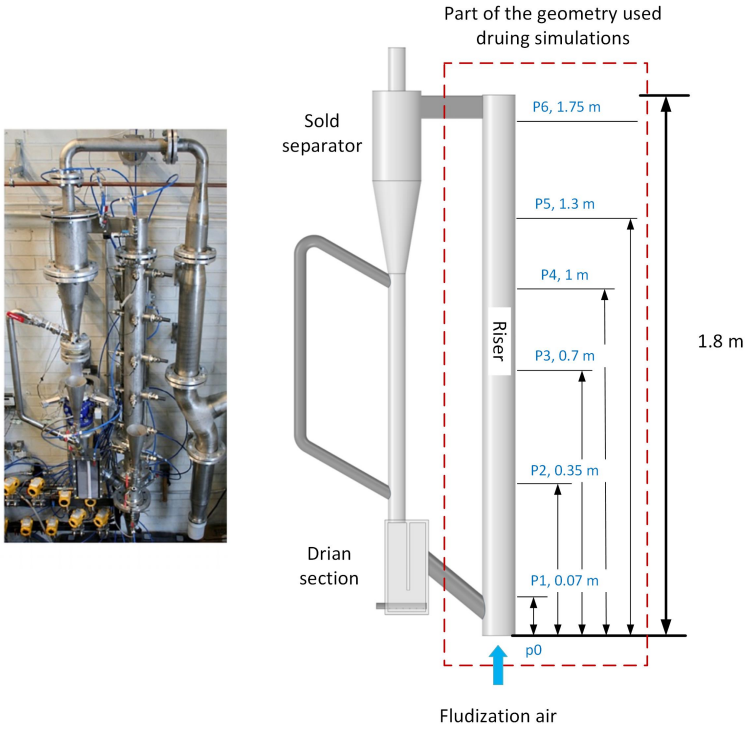

Figure 21: The pilot installation located at the Lappeenranta University of Technology [32] (left) and numerical mode with highlighted simplification and locations of the measurement ports

In order to simplify calculations, the geometry was modified. The following elements have been removed: loop-seal and drain section. As result the geometry used for calculations consists of the riser and two short pipes at the bottom and at the top as shown in a Fig. 22. The height of the riser is 1.8 m and its internal diameter equals to 0.11 m. The mesh consists of 38,450 hexahedral and tetrahedral elements with size of 0.01 m (Fig. 24). Measurement points of pressure are situated along the riser, starting from ground level at 0 m, 0.07 m, 0.35 m, 0.7 m, 1.0 m, 1.3 m, and 1.75 m.

Figure 22: Simplified mesh

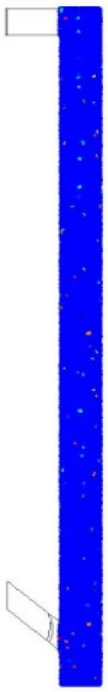

Figure 23: Part of pilot-scale rig used for injecting material

The experimental tests, together with DDPM simulations, were carried out in ambient conditions (cold). The mass of particle parcels in the domain amounts to 1 kg and gas velocity, introduced from the bottom of the riser, equals to 3.75 $\frac{\mathrm{m}}{\mathrm{s}}$. In the experiments glass particles, with the density of 2450 $\frac{\mathrm{kg}}{\mathrm{m}^3}$ were used. On the basis of 2d analysis particle diameters were determined. Particle diameter was ranging from 100 μm to 713 μm, the mean diameter was 513 μm, and the spread factor was determined to be equal to 9.13 based on Rossin-Rammler distribution [52].

To replace removed elements of a geometry a user defined function (UDF) was developed and implemented into the solution procedure. The general idea is to save, at the end of every time step, information about the number of particles and their mass which is leaving through the outlet of the domain. At the beginning of next time step, particle parcels with a total mass trapped previously are injected back to the riser through the recirculation surface (see Fig. 24). In general terms the number of streams injected back to the domain depends on number of faces composing a particular surface. The close up of a surface is also presented at Fig. 24. For this specific case the number of faces at the recirculation inlet surface is 80. Procedure of saving informations about the number of particle parcels and their mass leaving through the outlet, in order to inject back the same mass of solid phase, ensured the constant mass of the material in the domain.Results from the simulation of the flow in the riser using the DEM model will be validated with experiments, as well as with results obtained using the DDPM (Dense Discrete Phase Model) [52].

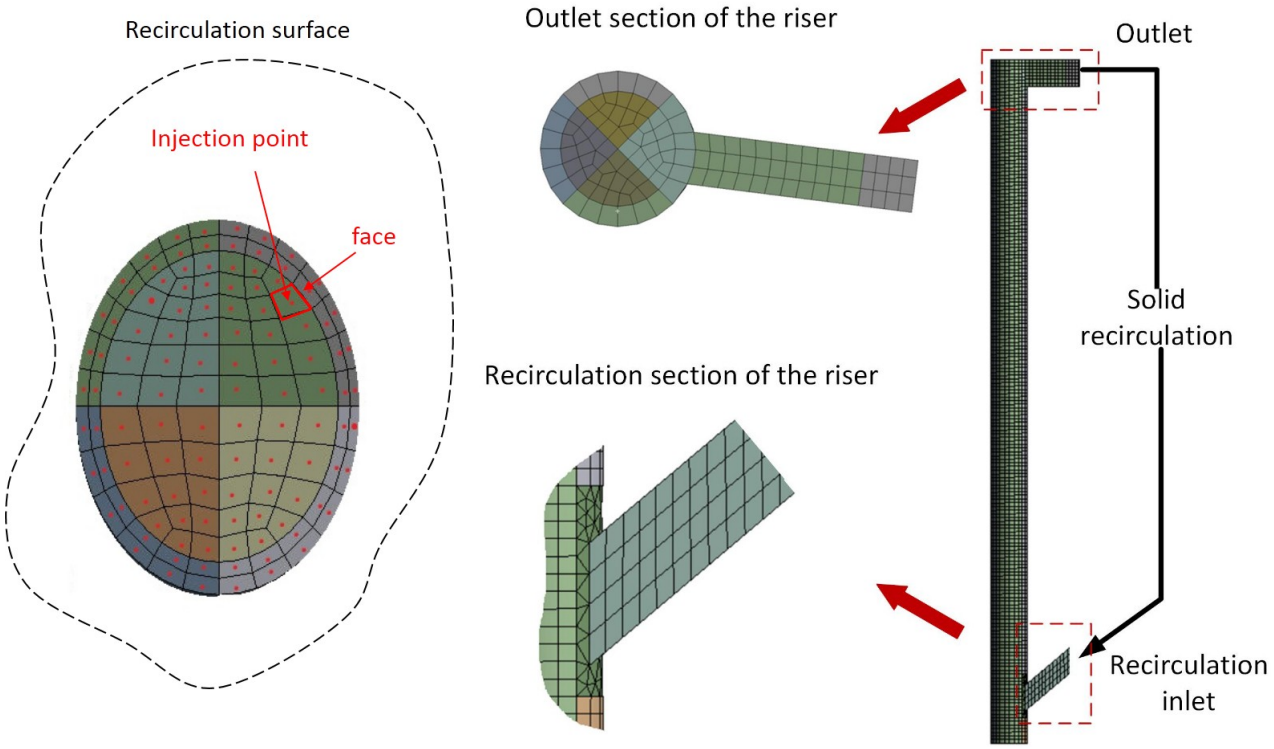

Figure 24: Recirculation scheme with close-up for recirculation surface

Using the DEM particles during interactions deform as shown at Fig. 6. The distance between particle parcel centers influences the collision force. The number of injection points is defined by the number of faces composing the surface and points are located in the middle of each face. The location of the particle parcel injection point at the beginning of the time step cannot be changed, therefore only one particle parcel diameter could be simulated at one time. Otherwise, to keep diversity in particle sizes few injection files would have to be assigned to one surface. It would result in the same position of injection points for different particles which would lead to unnatural overlapping (δ).Thus DEM simulations were conducted for three different cases, each with different particle diameter but constant mass of material in the riser (1.0 kg). Calculations were initialized by providing particle parcels into the riser. Three particle diameters ware tested, 275 μm, 325 μm, and 513 μm. For all cases the Gidaspow drag model was used to calculate interphase exchange coefficient (K). The number of parcels injected into the computational domain were 230,000, 135,000, and 75,000, respectively. To account for differences in particle diameters the different particle parcels diameters were set: 0.0015 m, 0.0018 m, 0.0022 m for particle parcel diameter equal to 275 μm, 325 μm, and 531 μm respectively.

5.2. Results

The results have been illustrated using the contours of solid volume fraction and pressure distribution in a pilot-scale rig. Pressure values, at different heights of the riser were gathered in table 6 together with results obtained in the experiments and results of modeling multiphase flow using DDPM. The changes of pressure and volume fractions are illustrated after 20 s of simulations. From the tenth second of simulations data sampling for time statistics was enabled to obtain values averaged in time.

Making use of gathered values of pressure, for visualizing results the figure 25 was created. Pressure values obtained from simulations using DEM are higher than experimental and DDPM data as shown at figure 25. The greatest difference can be noticed for the particle diameter 531 μm, for the smaller diameters the difference slightly decreases. For cases with smaller particle diameters (325 μm and 231 μm) dissimilarities in results are smaller because the particle parcel diameter is approaching the particle diameter. The forces resulting from collisions are weakened since the mass of the parcel is decreased. To obtain results similar to experimental values, it can be presumed that the parcel diameter should be equal to the particle diameter in such a way one parcel would contain only one particle. However, the calculation time would be extended due to increased number of particle parcels. Hence the probability of interparticle collisions would also be greater.

Due to wrongly predicted, exaggerated collision forces, the uniform distribution of the material in the riser occurs in a case with the biggest particle parcel diameter which can be seen in Fig. 26. Due to larger mass, parcels are reflecting from walls and each other constantly increasing energy. The obtained results are opposite to expected, whereas in a case with bigger particles they should accumulate at the bottom of the riser and only part of the material should occupy the top. Forces resulting from collisions are overpredicted, since the momentum is not calculated for the particle but for the parcel, which diameter is bigger. The decrease of the size of the parcel results in similar pressure values as the experimental data.

Table 6: Pressure measurements points

Measurement points, -	Height, m	Pressure, Pa				
		Experiment	DDPM	DEM		
				d=513um	d=325um	d=231um
1	0	1002.08	1076.45	1278.95	1281.91	1262.94
2	0.07	562.61	917.91	1209.33	1110.63	1078.90
3	0.35	348.93	518.16	991.80	677.58	668.26
4	0.7	216.77	317.80	735.62	497.83	488.05
5	1	141.12	210.19	519.72	373.65	363.71
6	1.3	75.98	122.14	307.72	246.80	237.26
7	1.75	0.00	0.00	0.00	0.00	0.00

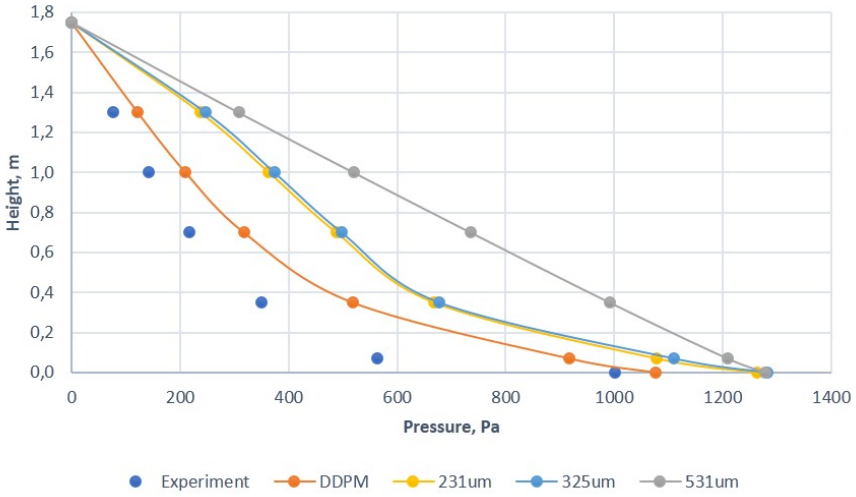

Figure 25: Time averaged pressures comparison for different cases

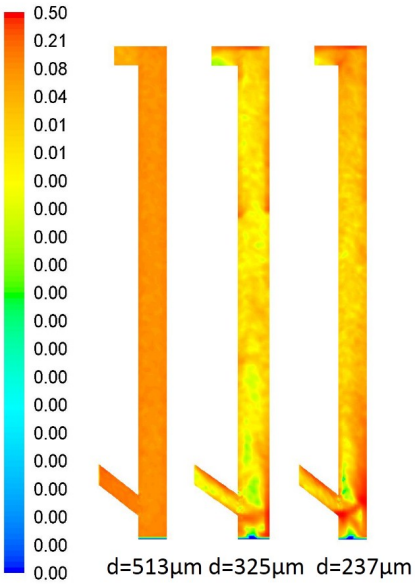

Figure 26: Averaged volume fraction distribution of phase 2 in pilot-scale rig

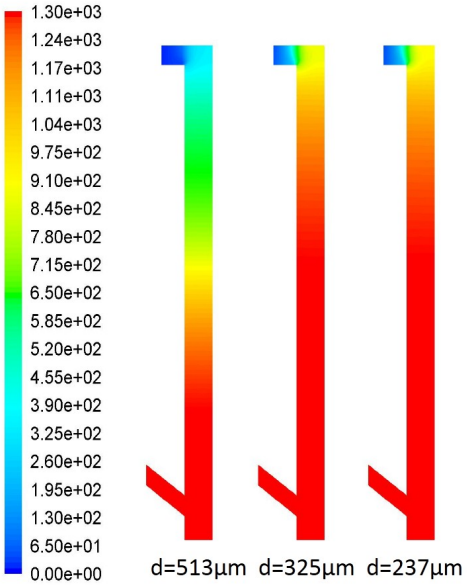

Figure 27: Pressure averaged distribution of phase 2 in pilot-scale rig

The obtained values were not satisfactory since large differences between measured and simulated data were observed. The observed issue is the wrongly predicted distribution of the material over the riser. It was expected that for larger size of the particle, the solid material will be accumulated at the bottom of the riser. By application of the spring deformation collisions model the interaction between particles cannot be accurately predicted. The model overpredicts the calculated forces and it is strongly sensitive to the mass, diameter and number of parcels within the computational domain. For instance, the drag force which acts on the parcel is

function of its diameter, rather than particle diameters. The application of the more sophisticated but direct colisional model like Herzian [4] should be used. Nevertheless, in case of using this model the simulation time is extremely long, which excludes its application for large scale applications. To better understand the behaviour of the model a simple case was designed. For this purpose the same geometrical model used for modeling combustion process depicted in Fig. 10 was used. The set of simulation was carried out for two particle diameters and two different values of tracked parcels, as shown in Tab. 7.

Table 7: Particle parcel diameter and number configuration

Number of particle parcels, -	Diameter of particle, um	Diameter of particle parcel, um
100,000	300	4.30
500,000	300	2.52
100,000	500	4.30
500,000	500	2.52

The contours of solid volume fraction and the particle distribution, are shown in Fig. 28 and Fig. 29 respectively. The mentioned effects can be easily recognized in illustrated figures. The case of particle diameter equal to 300 μm, it can be seen that increasing the number of parcels in the computational domain the parcel and mass of the parcel is reduced. In consequence parcels are intensively mixed and due to the predicted forces, not only concessional but also drag material are transported to higher sections of the computational domain. The identical feature can be observed for the second particle size.

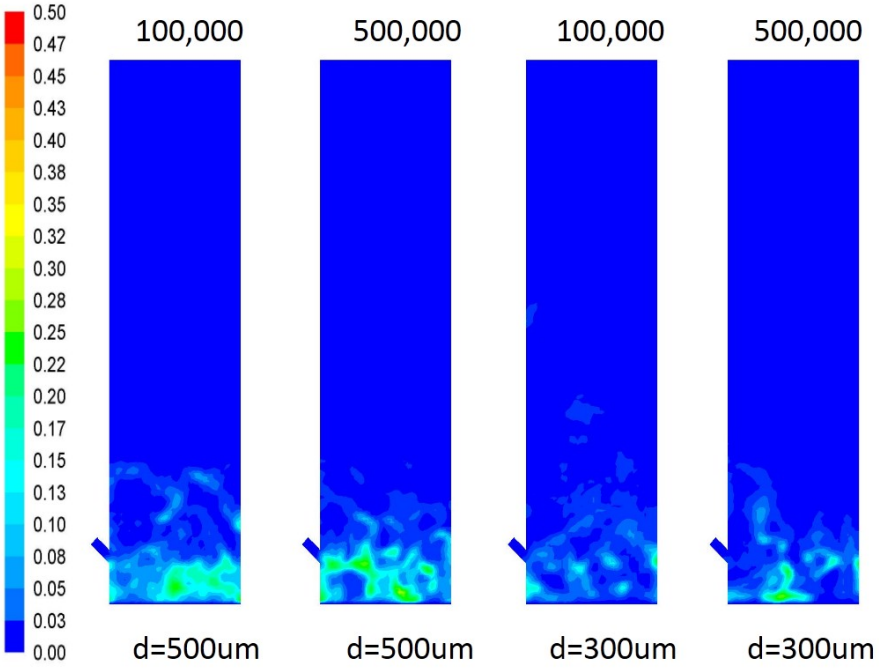

Figure 28: Volume fraction of cases with different number of particle parcels

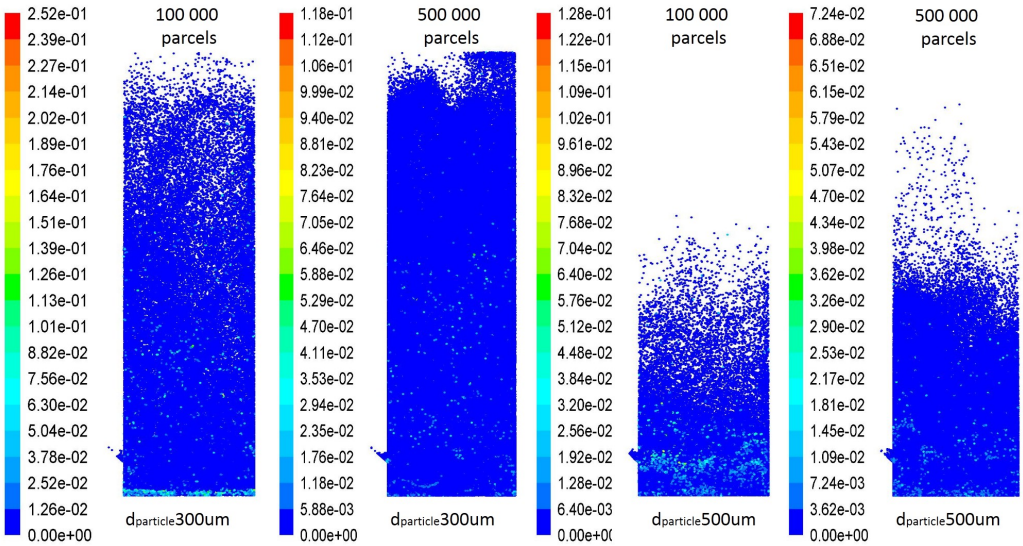

Figure 29: Particle parcel distribution colored by collision force magnitude

6. Conclusions

The work was divided into two parts: simulations of heat transfer together with combustion and modeling multiphase flow in a pilot scale CFB testing rig. For this purpose the commercial code Ansys Fluent was used. For predicting interparticle collisions DEM was applied, as the main goal of the thesis was to check and investigate if it is applicable to such problems. The temperature, CO_2 content in flue gases, volume fraction of solid phase and particle distribution in a domain with changes in its temperature were discussed.

In the first part, by not having experimental results, analythical calculations were made to check global mass and energy conservation from simulations. Comparing temperature of injected sand particles, while only hot gas was flowing through domain, the values obtained both from Ansys Fluent and external source gave similar values (temperature rise of 10 K). Small value called into question if DEM model do not taint results. After further investigations and additional calculations it was found that heat transfer is not calculated for single particle but for a parcel composed of particles (in order to decrease computational cost). If the parcel had the diameter/mass of a single particle, the increase in temperature would be higher than 410 K.

Furthermore, the results obtained from simulating combustion of coal in a combustion chamber almost covered with external calculations. Temperature distribution as well as CO_2 mass fraction was uniform in a domain where two air inlets were created but still results were similar to case with only one side inlet of fuel. At the outlet concentration of flue gas compounds was slightly lower in domain with two side ports. Taking advantage of applying UDF, that allowed nipping mass of char and ash off at the outlet of a domain the energy balance was calculated. For both cases similar value of energy absorbed by a sand to increase its temperature was obtained. Even though two variants can be treated as good solution, it leans towards applying two inlets of fuel to a chamber since results stabilize faster.

In the second part, a trial to simulate multiphase flow through a pilot-scale test rig. Results of calculations diverged from experimental and DDPM values. Pressure distribution did not followed volume fraction of the solid phase in domain. Pressure rised from the bottom through the top while the volume fraction of the solid

phase was biggest at the bottom and on the top, diluted in the middle of the riser. Assumed at the beginning that only for simulations particle parcels are created in order to simplify calculations, not influencing the results of collisions between particles. Throughout additional simulations, it was found out that similarly to heat transfer between particles also momentum is calculated for the particle parcel. To obtain exact results of interparticle interactions the particle parcel should contain only one particle inside, so is have the same diameter as particle itself.

The DEM model remains computationally the most expensive among available approaches namely Euler-Euler, Euler-Lagrange. Simulations predicting direct interparticle parcels collisions took for the first part of thesis 4-5 days and for the second part 3 weeks. However, it was proven that DEM can be used for modeling combustion process in small scale as well as heat transfer itself. Given results were reliable and proved by set of calculations. Has to be remembered that for obtaining exact results of inter particulates forces parcel should contain only one particle for providing the same diameter for both of them. Also DEM model is very sensitive if it is to overlapping of particles and therefore big collision forces acting on particles, as a result giving uneven distribution of particles and their unnatural behaviour. Given solutions persists that DEM is the most demanding model from all mentioned in thesis.

Future work will be focused on replacing the standard KTGF and DEM collision approaches used in hybrid Euler-Lagrange technique for prediction particle interactions by development of a reduced order Surrogate Model. The goal will be to determine collisional acceleration force (F_{col}) for individual parcels (F^{p}_{col}) based on the micro-scale DEM approach, where collisions will be predicted based on the Soft Sphere Model. In the proposed approach the unstable, expensive KTGF interaction model can be simply skipped. Surrogate Model will predicts this forces using combination of space dependent modes (Properly Orthogonally Decomposed base) calculated for a wide range of input parameters (number of particles, their velocity components, number of particle in cell, mechanical properties, etc.).

[1] A. Szlek, R. Wilk, S. Werle, N. Schaffel, Czyste technologie pozyskiwania energii z wegla oraz prespektywy bezplomieniowego spalania, Rynek spalania 25 (2009) 100–110.

[2] P. Palamarczuk, J. Konieczynski, Ekologiczne walory stosowania kotlow fluidalnych w sektorze komunalnym, Prace Naukowe GiG Gornictwo i Srodowisko 3 (2005) 99–118.

[3] Y. Zhang, L. Qinghai, Z. Hui, Theory and calculation of heat transfer in furnaces, 1st Edition, Academic Press, 2016.

[4] C. Crowe, J. Schwarzkopf, M. Sommerfeld, Y. Tsuji, Multiphase flows with droplets and particles, Taylor & Francis Group, 2012.

[5] W. Oing, B. Jingru, Z. Lixia, S. Baizhong, L. Hongpeng, Validity of an expert system for oil shale-fired CFB boiler design and performance analysis, Oil Shale 25 (2008) 400–411.

[6] K. Nuortimo, State of the art cfb technology for flexible large scale utility power production (March 2015).
URL http://www.amecfw.fr/documents/downloads/technical-papers/state-of-the-art\
\-cfb-technology-utility-power-production.pdf

[7] H. Topal, Y. Altinsoy, O. Erbas, Des ign and application of automatic control system in a laboratory scale fluidized bed coal combustion system, Journal of Science 5(2) (2018) 49–63.

[8] S. Ergun, Fluid flow through packed columns, Chemical Engineering Progress 48 (1952) 89–94.

[9] D. Gidaspow, Multiphase flow and fluidization, Academic Press, 1994.

[10] J. Paska, M. Salek, T. Surma, Wywarzanie energii elektrycznej z wykorzystaniem odnawialnych zasobow energii (March 2005).
URL https://www.cire.pl/pliki/2/wyklad2.pdf

[11] P. Korasiak, Sprawnosc konwersji promieniowania slonecznego na energie elektryczna wspolczesnych ogniw i modulow fotowoltaicznych (March 2017).
URL http://pe.org.pl/articles/2017/7/27.pdf

[12] X. Chen, J. Wang, A comparison of two-fluid model, dense discrete particle model and CFD-DEM method for modeling impinging gas–solid flows, Powder Technology 254 (2014) 94–102.

[13] M. Farid, H. Jeong, K. Kim, J. Lee, D. Kim, J. Hwang, Numerical investigation of particle transport hydrodynamics and coal combustion in an industrial-scale circulating fluidized bed combustor: effects of coal feeder positions and coal feeding rates, Fuel 192 (2017) 187–202.

[14] W. Adamczyk, K. Myöhänen, E. Hartge, J. Ritvanen, A. Klimanek, T. Hyppänen, R. Bialecki, Generation of data sets for semi-empirical models of circulated fluidized bed boilers using hybrid Euler-Lagrange technique, Energy 143 (2018) 219–240.

[15] K. Myohanen, T. Hyppanen, A three-dimensional model frame for modelling combustion and gasification in circulating fluidized bed furnaces, International Journal of Chemical Reactor Engineering 9(25) (2011) 55.

[16] D. Gera, M. Gautam, Y. Tsuji, T. Kawaguchi, T. Tanaka, Computer simulation of bubbles in large-particle fluidized beds, Powder Technology 98 (1998) 38–47.

[17] D. Gidaspow, V. Jiradilok, Computational techniques, the multiphase CFD approach to fluidization and green energy technologies, 1st Edition, Nova Science Publishers, Inc., 2009.

[18] T. Anderson, R. Jackson, A fluid mechanical description of fluidized beds equations of motion, Industrial & Engineering Chemistry Fundamentals 6 (1967) 527–539.

[19] S. Chapman, T. Cowling, The mathematical theory of non-uniform gases, 3rd Edition, Cambridge Univ. Press, 1970.

[20] M. Syamlal, W. Rogers, O. T.J., MFIX Documentation, National Technical Information Service 1 (1993) 5540–5551.

[21] B. Hoomans, J. Kuipers, W. Briels, W. Swaaij, Discrete particle simulation of bubble and slug formation in a two-dimensional gas-fluidized bed: A hard-sphere approach, Chemical Engineering Science 51 (1996) 99–118.

[22] Y. Tsuji, T. Kawaguchi, T. Tanaka, Discrete particle simulation of two-dimensional fluidized bed, Powder Technology 77 (1996) 79–87.

[23] H. Zhou, G. Flamant, D. Gauthier, J. Lu, Lagrangian approach for simulating the gas-particle flow structure in a circulating fluidized bed riser, International Journal of Multiphase Flow 28 (2002) 1801–1821.

[24] T. Tsuji, K. Yabumoto, T. Tanaka, Spontaneous structures in three-dimensional bubbling gas-fluidized bed by parallel DEM-CFD coupling simulation, Powder Technology 184 (2008) 132–140.

[25] M. Andrews, P. O'Rourke, The multifluid particle-in-cell (MP-PIC) method for dense particulate flows, International Journal of Multiphase Flow 22 (2) (1996) 379–402.

[26] N. Patankar, D. Joseph, Lagrangian numerical simulation of particulate flows, International Journal of Multiphase Flow 27 (10) (2001) 1685–1706.

[27] N. Patankar, D. Joseph, Modeling and numerical simulation of particulate flows by the Eulerian-Lagrangian approach, International Journal of Multiphase Flow 27 (10) (2001) 1659–1684.

[28] D. Snider, P. O'Rourke, M. Andrews, Sediment flow in inclined vessels calculated using a multiphase particle-in-cell model for dense particle flows, International Journal of Multiphase Flow 24 (1998) 1359–1382.

[29] D. Snider, An incompressible three-dimensional multiphase particle-in-cell model for dense particle flows, Journal of Computational Physics 170 (2001) 523–549.

[30] D.M. Snider and S. Banerjee, Heterogeneous gas chemistry in the CPFD Eulerian–Lagrangian numerical scheme (ozone decomposition), Powder Technology 199 (2010) 100—106.

[31] A. Klimanek, W. Adamczyk, A. Katelbach-Wozniak, G. Wecel, A. Szlek, Towards a hybrid Eulerian–Lagrangian CFD modeling of coal gasification in a circulating fluidized bed reactor, Fuel 152 (2015) 131–137.

[32] M. Nikku, P. Jalali, T. Hyppänen, Comparison of Ansys Fluent and OpenFoam in simulation of circulating fluidized bed riser., 12th International Conference on Fluidized Bed Technology 62 (2016) 100–111.

[33] I. ANSYS, ANSYS Fluent On-line: http://www.ansys.com.

[34] M. Andrews, P. O'Rourke, The multifluid particle-in-cell (MP-PIC) method for dense particulate flows, International Journal of Multiphase Flow 22 (2) (1996) 379–402.

[35] M. Syamlal, W. Rogers, T. O'Brien, Equilibrium Land Use Patterns In A Nonmometr City (December 1993).
URL `http://www.mfix.org(2007-04-15)`

[36] D. Schaeffer, Instability in the evolution equations describing incompressible granular flow, Journal of Differential Equation 66 (1987) 19–50.

[37] C. Lun, S. Savage, D. Jeffrey, N. Chepurnly, Kinetic theories for granular flow: inelastic particles in couette flow and slightly inelastic particles in a general flow field, Journal Fluid Mechanics 140 (1984) 223–256.

[38] S. Ergun, Fluid flow through packed columns, Chemical Engineering Progress 48 (2) (1952) 89–94.

[39] C. Wen, Y. Yu, Mechanics of fluidization, Chemical Engineering Progress Symposium Series 62 (1966) 100–111.

[40] H. L., G. D., Hydrodynamics of binary fluidization in a riser: CFD simulation using two granular temperatures, Chemical Engineering Science 58 (2003) 3777–3792.

[41] I. Goldhirsch, Introduction to granular temperature, Powder Technology 182 (2008) 130–136.

[42] B. V. Wachem, J. Schouten, C. V. den Blee, R. Krishn, J. Sinclair, Comparative analysis of CFD models of dense gassolid systems, AIChE Journal 47 (5) (2001) 1035–1051.

[43] D. Gera, M. Gautam, Y. Tsuji, T. Kawaguchi, T. Tanaka, Computer simulation of bubbles in large-particle fluidized beds, Powder Technology 98 (1998) 38–47.

[44] P. Cundall, O. Strack, A discrete element model for granular assemblies, Géotechnique, 1979.

[45] J. Lucas, Force, mass acceleration: Newton's Second Law of motion.
URL `https://www.livescience.com/46560-newton-second-law.html`

[46] J. Szargut, Termodynamika techniczna, Wydawnictwo Politechniki Slaskiej, 2003.

[47] B. Jagustyn, N. Batorek-Giesa, B. Wilk, Ocena wlasciwosci biomasy wykorzystywanej do celow energetycznych, Chemik 65 (6) (2011) 557–563.

[48] H. Groenewold, E. Tsotsas, Predicting apparent sherwood numbers for fluidized beds, Drying Technology 17(7-8) (1999) 1557–1570.

[49] I. Glassman, R. A. Yetter, N. G. Glumac, Combustion of nonvolatile fuels, Combustion (5th Edition) (2015) 477–536.

[50] S. Badzioch, P. Hawksley, Kinetic of thermal decomposition of pulverized coal particles, Industrial and Engineering Chemistry Process Design and Development 9 (4) (1970) 521–530.

[51] M. Baum, P. Street, Predicting the combustion behavior of coal particles, Combustion Science Technology 3 (5) (1971) 231–243.

[52] A. Bartoszewicz, Hybrid Euler-Lagrange approach for modelling transport phenomena in a laboratory CFB unit, Wydawnictwo Politechniki Slaskiej 2018.